

This discussion paper is/has been under review for the journal Atmospheric Chemistry and Physics (ACP). Please refer to the corresponding final paper in ACP if available.

Balloon-borne match measurements

A. Cirisan et al.

Balloon-borne match measurements of mid-latitude cirrus clouds

A. Cirisan¹, B. P. Luo¹, I. Engel¹, F. G. Wienhold¹, U. K. Krieger¹, U. Weers¹, G. Romanens², G. Levrat², P. Jeannet², D. Ruffieux², R. Philipona², B. Calpini², P. Spichtinger³, and T. Peter¹

¹Atmospheric and Climate Science, ETH Zurich, Zurich, Switzerland

²Federal Office of Meteorology and Climatology MeteoSwiss, Chemin de l'Aérologie, Payerne, Switzerland

³Institute for Atmospheric Physics, Johannes Gutenberg University Mainz, Mainz, Germany

Received: 16 July 2013 – Accepted: 25 August 2013 – Published: 2 October 2013

Correspondence to: A. Cirisan (ana.cirisan@alumni.ethz.ch)

Published by Copernicus Publications on behalf of the European Geosciences Union.

Title Page

Abstract

Introduction

Conclusions

References

Tables

Figures

◀

▶

◀

▶

Back

Close

Full Screen / Esc

Printer-friendly Version

Interactive Discussion



Abstract

Observations of persistent high supersaturations with respect to ice inside cirrus clouds are challenging our understanding of cloud microphysics and of climate feedback processes in the upper troposphere. Single measurements of a cloudy air mass provide only a snapshot from which the persistence of ice supersaturation cannot be judged. We introduce here the “cirrus match technique” to obtain information of the evolution of clouds and their saturation ratio. The aim of these coordinated balloon soundings is to analyze the same air mass twice. To this end the standard radiosonde equipment is complemented by a frost point hygrometer “SnowWhite” and a particle backscatter detector “COBALD” (Compact Optical Backscatter Aerosol Detector). Extensive trajectory calculations based on regional weather model COSMO forecasts are performed for flight planning and COSMO analyses are used as basis for comprehensive microphysical box modeling (with grid scale 2 km and 7 km, respectively). Here we present the results of matching a cirrus cloud to within 2–15 km, realized on 8 June 2010 over Payerne, Switzerland, and a location 120 km downstream close to Zurich. A thick cirrus was detected over both measurement sites. We show that in order to quantitatively reproduce the measured particle backscatter ratios, the small-scale temperature fluctuations not resolved by COSMO must be superimposed on the trajectories. The stochastic nature of the fluctuations is captured by ensemble calculations. Possibilities for further improvements in the agreement with the measured backscatter data are investigated by assuming a very slow mass accommodation of water on ice, the presence of heterogeneous ice nuclei, or a wide span of (spheroidal) particle shapes. However, the resulting improvements from microphysical refinements are moderate and comparable in magnitude with changes caused by assuming different regimes of temperature fluctuations for clear sky or cloudy sky conditions, highlighting the importance of a proper treatment of subscale fluctuations. The model yields good agreement with the measured backscatter over both sites and reproduces the measured saturation ratios with respect to ice over Payerne. Conversely, the 30 % in-cloud supersaturation measured

Balloon-borne match measurements

A. Cirisan et al.

Title Page

Abstract

Introduction

Conclusions

References

Tables

Figures

◀

▶

◀

▶

Back

Close

Full Screen / Esc

Printer-friendly Version

Interactive Discussion



in a massive, 4-km thick cloud layer over Zurich cannot be reproduced, irrespective of the choice of meteorological or microphysical model parameters. The measured supersaturation can only be explained by either resorting to an unknown physical process, which prevents the ice particles from consuming the excess humidity, or - much more likely - by a measurement error, such as a contamination of the sensor housing of the SnowWhite hygrometer by a precipitation drop from a mixed phase cloud just below the cirrus layer or from some very slight rain in the boundary layer. This uncertainty calls for in-flight checks or calibrations of hygrometers under the extreme humidity conditions in the upper troposphere.

1 Introduction

Cirrus clouds play an important role in the complex mechanisms of climate change (Solomon et al., 2007). Their ability to reflect, transmit and absorb solar radiation and to absorb and emit infrared terrestrial radiation impacts the terrestrial radiation balance (Mason, 2002). Depending on optical thickness and altitude, and on the albedo of the surface or the lower clouds, the net effect on climate can either be a cooling or warming (Chen et al., 2000; Fusina et al., 2007; Corti and Peter, 2009), but quantifying the magnitude of this effect is difficult because of uncertainties in these or other quantities characterizing the cirrus life cycle (Lynch et al., 2002). Furthermore, microphysical properties such as number density, size and shape of the ice crystals affect the cloud lifetime and radiative properties and thus the humidity of the upper troposphere and lower stratosphere (Jensen and Toon, 1994).

The formation and evolution of cirrus clouds depends strongly on environmental conditions (temperature, cooling rate, relative humidity, wind field etc.), cloud internal dynamics (Marshall and Dobbie, 2005; Fusina and Spichtinger, 2010), as well as on background aerosols that are either liquid and freeze homogeneously (Hoyle et al., 2005; Spichtinger and Gierens, 2009a) or contain a solid and may act as heterogeneous ice nuclei (DeMott et al., 2010). Ice in the upper troposphere is known to nu-

Title Page

Abstract

Introduction

Conclusions

References

Tables

Figures

◀

▶

◀

▶

Back

Close

Full Screen / Esc

Printer-friendly Version

Interactive Discussion



Balloon-borne match measurements

A. Cirisan et al.

Title Page

Abstract

Introduction

Conclusions

References

Tables

Figures

◀

▶

◀

▶

Back

Close

Full Screen / Esc

Printer-friendly Version

Interactive Discussion



create via both pathways, homogeneous freezing of aqueous solution droplets (Koop et al., 2000) or heterogeneous nucleation on solid aerosol particles (DeMott et al., 2003). Both mechanisms, and especially homogeneous freezing, require regions with very low temperatures and high supersaturation with respect to ice. Ice supersaturated regions (ISSRs), i.e. clear air masses with ice supersaturation, are the potential formation regions for cirrus clouds (Gierens and Spichtinger, 2000; Spichtinger et al., 2003a, b). A variety of data sets (satellite, aircraft, radiosondes) and trajectory calculations serve to improve the understanding of ISSRs and cirrus formation (Ovarlez et al., 2000; Comstock et al., 2004; Jensen et al., 2005; Spichtinger et al., 2005; Gettelman et al., 2006; Vömel et al., 2007; Krämer et al., 2009). Although persistent ISSRs in the upper tropospheric cloud-free air are well understood, very high in-cloud supersaturations are difficult to comprehend, since ice crystals should readily deplete the supersaturated water vapour leading to a fast decrease of supersaturation. Even though several potential theoretical explanations for persistent supersaturations have been alluded to, this phenomenon and the frequency of its occurrence remain difficult to understand (Peter et al., 2006, 2008). As shown by the hygrometer intercomparison campaign AquaVIT (Fahey et al., 2009), instrumental artifacts may also cause some of the observed massive supersaturations: under static cloud-free conditions a core group of eight water vapour instruments investigated by AquaVIT were generally within $\pm 10\%$ of a reference value for water mixing ratios > 10 ppmv (and total air pressures 70–500 hPa), with some outliers up to $\pm 20\%$. This translates into an uncertainty in relative humidity with respect to ice, RH_{ice} , of 10–20%. While these results prove that significant discrepancies between instruments exist, they were obtained under well controlled static conditions, which differs from conditions in the field (e.g., because of reduced ventilation of the instruments).

Humidity measurements inside cloud-free ISSRs or cirrus clouds provide normally only an Eulerian measurement, i.e. a snapshot of the investigated air mass. In order to investigate their temporal evolution, a Lagrangian element was introduced in sonde measurements and modeling within the framework of the project LAMMOC (LA-

grangian Measurements and MOdeling of Cirrus clouds). The main idea of the project was to analyze and understand the life cycle of cirrus clouds in mid-latitude regions as well as the occurrence and evolution of RH_{ice} inside these clouds by measuring the same air parcels twice within a few hours. Here we discuss balloon-borne cirrus particle backscatter and relative humidity measurements using this so-called “match” technique. The MeteoSwiss radio-sounding site at Payerne (46.813° N and 6.943° E) was taken as a fixed starting point for one of the two “match” soundings. A mobile balloon-sounding unit was then used to launch a second radiosonde about 2 h later downstream of Payerne within the greater area of Zurich. The aim to measure the same air mass at cirrus level twice by two subsequent soundings is ambitious and in order to fully account for the Lagrangian point of view, intensive trajectory calculations have been performed for flight planning and analysis. Microphysical box modeling was used to reproduce the atmospheric profiles for the measurement period (starting a few hours upstream) in order to understand the formation and evolution of the observed cirrus cloud.

2 “Match” technique

The idea for this technique was first coined during ozone loss studies in the Arctic (Rex, 1993; von der Gathen et al., 1995). Within the framework of the European Arctic Stratospheric Ozone Experiment (EASOE), ozone depletion rates were calculated from matches between random balloon soundings, thereby following the evolution of ozone along the trajectories inside the polar vortex. Rex et al. (1997, 1999) improved the technique using numerical weather forecast models as tool for air parcel tracking and predicting the optimum time for the launch of the second balloon sonde. During the SOLVE/THESEO-2000 Arctic stratospheric campaign in the winter 1999/2000, Fueglistaler et al. (2002) applied the match technique to trace widespread occurrences of very large HNO_3 -containing particles in very low number densities, probably composed of nitric acid trihydrate (NAT), back to Polar Stratospheric Clouds (PSCs) with

Balloon-borne match measurements

A. Cirisan et al.

Title Page

Abstract

Introduction

Conclusions

References

Tables

Figures

◀

▶

◀

▶

Back

Close

Full Screen / Esc

Printer-friendly Version

Interactive Discussion



Balloon-borne match measurements

A. Cirisan et al.

[Title Page](#)[Abstract](#)[Introduction](#)[Conclusions](#)[References](#)[Tables](#)[Figures](#)[◀](#)[▶](#)[◀](#)[▶](#)[Back](#)[Close](#)[Full Screen / Esc](#)[Printer-friendly Version](#)[Interactive Discussion](#)

higher number densities occurring on the mesoscale. Using forward trajectories, they were able to connect the mesoscale “mother clouds” to low number density NAT particle populations several days downstream. Lagrangian characterization of air parcels in order to quantify the efficiency of dehydration in the tropical tropopause layer (TTL) over the western Pacific was conducted as part of the Soundings of Ozone and Water in the Equatorial Region (SOWER) project using frost point hygrometers (Hasebe et al., 2007; Inai, 2010). The water vapour match determined from the SOWER network observations was chosen based on isentropic trajectories calculated from the ECMWF operational analysis data, fulfilling temperature and ozone mixing ratio criteria. And finally, Dionisi et al. (2013) used the match method to estimate cirrus crystal fall velocity from ground-based lidar observations. Several attempts to investigate the temporal evolution of cirrus clouds during the aircraft campaigns (Gultepe and Starr, 1995; Field et al., 2006) and using satellite measurements (Soden, 2004) reveal how challenging the Lagrangian measurements are.

In the present work we perform the probably first balloon-borne cirrus match study over mid-latitudes. Favourable cirrus match conditions are determined from the following criteria. The balloon launch requires a general alignment of the wind direction as the first criterion, in order to minimize the travel distance of the mobile equipment for the downstream measurement. Secondly, a forecast relative humidity with respect to ice exceeding 90% in the cirrus altitude region is demanded as an prerequisite of cloud existence. Thirdly, the wind speed needs to be sufficiently small to allow for at least one hour time between the two launches in order to observe possible changes in supersaturation within the air mass. As a final criterion, wind shear must be sufficiently small.

Extended ice supersaturated regions ($RH_{ice} > 90\%$) and cirrus clouds (ice water content $IWC > 10$ mg H_2O/kg air) are determined using nested Consortium for Small-Scale Modeling (COSMO) / European Centre for Medium-Range Weather Forecasts (ECMWF) forecasts. The localization of the downstream match point is based on forecasts from COSMO-2, i.e. the 2-km resolution version of the regional weather forecast

model COSMO, which we retrieved every 3 h. By means of trajectory ensemble calculations based on the COSMO-2 forecasts, we investigated whether match radii better than 10 km could be reached in the layer relevant for cirrus formation.

The two matching balloon soundings are established as follows (compare Fig. 1):

- (a) Flight trajectory of the upstream radiosonde: The ascent flight path of the first balloon is simulated as forward trajectory by superimposing a fixed 5 ms^{-1} climb rate onto the COSMO wind field in order to obtain the position of the radiosonde at cirrus altitude.
- (b) Ensemble of air parcel trajectories: Positions along the upstream radiosonde flight path are determined at 15 altitudes with a spacing of 300 m in the 6–12 km height range. From these points air parcel forward trajectories are calculated.
- (c) Flight trajectory of the downstream radiosonde: For each of the 15 air parcel trajectories the backwards balloon trajectories (with superimposed -5 ms^{-1} climb rate) are calculated to obtain the potential launch site and time.
- (d) Match quality at higher levels: Forward balloon trajectories are then calculated from the potential downstream launch determined under (3) to estimate the match quality at higher levels. The launch site is selected according to optimized humidity conditions and “match” distances (calculated between the potential second balloon ascent and the given air parcel trajectories on isentropic surfaces).

For the preselected altitude the match distance is zero according to the forecast, while above and below this altitude the match worsens due to wind shear. After the flight the calculations are repeated with meteorological analysis instead of forecast data and with the actual balloon track as recorded by GPS, showing that the preselected match is typically off by 3 or 4 km.

Balloon-borne match measurements

A. Cirisan et al.

Title Page

Abstract

Introduction

Conclusions

References

Tables

Figures

◀

▶

◀

▶

Back

Close

Full Screen / Esc

Printer-friendly Version

Interactive Discussion



3 Instruments and models

The experimental setup consisted of two standard MeteoSwiss balloon radiosondes (Meteolabor SRS C-34, type 64, serial numbers: Payerne 18651, Zurich 17654) carrying the payload of approximately 1800 g. It comprised a SnowWhite hygrometer (from
5 Meteolabor, Switzerland), a COBALD particle backscatter sonde (our own development), and in addition the standard Rotronic HC2 Humicap capacitive polymer sensor and global positioning system (GPS) receiver. Meteorological parameters measured by these radiosondes are temperature, pressure, and wind extracted from the GPS data. The balloons have typical mean ascent rates of about 5 ms^{-1} , reaching altitudes
10 between 30 km to 35 km before burst. During descent, the payload is attached to a parachute, allowing for a potential recovery.

3.1 COBALD particle backscatter sonde

The lightweight Compact Optical Backscatter Aerosol Detector (COBALD) was developed recently at Swiss Federal Institute of Technology (ETH Zurich) to be flown on
15 operational weather balloons (Wienhold, 2012). It has specifications comparable to the Wyoming backscatter sonde by Rosen and Kjome (1991), but implementing high power light emitting diodes (LEDs) replacing the flashlamp. COBALD is much lighter (500 g including batteries) than the Rosen & Kjome sonde (6 kg). The two LEDs emit light at 455 nm (blue) and 870 nm (infrared). A silicon detector detects the light, backscattered
20 by air molecules, aerosols or cloud particles and allows signal retrieval at a higher frequency (1–20 Hz) than the Rosen and Kjome sonde (0.15 Hz). Daylight saturates the photo-detector and therefore COBALD measurements are only carried out at night. COBALD data analysis provides the backscatter ratio (BSR), which is defined as the net signal (from molecules and aerosol particles) divided by the Rayleigh signal (air
25 pure molecular scattering and the BSR is close to unity. The aerosol backscatter ratio

Balloon-borne match measurements

A. Cirisan et al.

[Title Page](#)[Abstract](#)[Introduction](#)[Conclusions](#)[References](#)[Tables](#)[Figures](#)[◀](#)[▶](#)[◀](#)[▶](#)[Back](#)[Close](#)[Full Screen / Esc](#)[Printer-friendly Version](#)[Interactive Discussion](#)

3.3 Numerical weather prediction models and trajectory calculations

For air parcel and balloon trajectory calculations a standard tool for Lagrangian investigations developed at ETH Zurich is used. The Lagrangian Analysis Tool (LAGRANTO, Wernli and Davies (1997)), originally based on ECMWF wind fields, was adapted to the output of the regional Numerical Weather Prediction (NWP) model COSMO for air trajectories and to routines for the balloon trajectory model (Engel, 2009). ECMWF forecasts give a prediction with a horizontal resolution of 25 km, reaching 80 km altitude with 91 levels. COSMO-2 provides a 24 h forecast for match sounding with the horizontal resolution of 2.2 km and 60 levels in vertical, reaching an altitude of approximately 23 km. With the same vertical spacing but 6.6 km horizontal resolution, COSMO-7 runs are performed for the following 48 h using a 72 h forecast. Forecasts longer than three days are provided by ECMWF and used as lateral boundary conditions for the nested COSMO-7. Values are obtained every minute along each trajectory or pathway of a balloon flight for latitude, longitude, altitude, pressure, temperature, potential temperature, water vapour mixing ratio, relative humidity with respect to ice, liquid and ice water content, wind speed and wind direction.

3.4 Ice microphysics scheme

The comprehensive Zurich spectral optical and microphysical Lagrangian box model (ZOMM) was used to perform detailed microphysical analysis in order to simulate the formation and evolution processes of the observed cloud. This model has been applied previously for polar stratospheric cloud investigations and tropospheric aerosol and cirrus studies (Luo et al., 2003; Hoyle et al., 2005; Engel et al., 2013). It is also used as a column model, driven by temperature and pressure data along staggered air parcel trajectories (Brabec et al., 2012), and in the present context we will make use of this column feature. Kinetically limited uptake or release of water by ice and aqueous $(\text{NH}_4)_2\text{SO}_4$ and H_2SO_4 solution droplets as well as the ice nucleation of liquid aerosol particles are treated in detail in a Lagrangian approach, i.e. by moving particles

Balloon-borne match measurements

A. Cirisan et al.

Title Page

Abstract

Introduction

Conclusions

References

Tables

Figures

◀

▶

◀

▶

Back

Close

Full Screen / Esc

Printer-friendly Version

Interactive Discussion



microphysical model into a simulated backscatter sonde signal along the chosen trajectory. The information from the microphysical scheme is used as input for the optical model, which allows to calculate backscatter coefficients and depolarization ratios of particles at arbitrary wavelengths, here in particular at the COBALD wavelengths. By comparing the results of the optical simulation with the observed BSR, certain parameters of the microphysical model can be constrained. The scattering matrix of liquid particles is computed exactly by solving the scattering problem by means of Mie theory (Bohren and Huffman, 2010). The refractive index of the aqueous droplets is calculated using the model of Krieger et al. (2000) for $\text{H}_2\text{SO}_4\text{-H}_2\text{O}$ solution droplets. For the calculation of the backscattering by ice particles we use the refractive index of ice (1.31) and apply the T-matrix method by Mishchenko (1991) to estimate shape effects. Here, we approximate the ice particles by prolate (“cigar-like”) spheroids with the aspect ratio $A = a/b$ (the ratio of the equatorial to polar lengths) and volume $V = 4/3\pi a^2 b$, which is taken equal to the volume of the ice particles calculated by the microphysical model. Following Brabec et al. (2012), we assume an aspect ratio $A = 0.75$, i.e. slightly prolate, which may be a typical value for midlatitude cirrus cloud particles. Nousiainen and McFarquhar (2004) found that the small ice crystals with dimension $< 100\ \mu\text{m}$ are mostly quasi-spherical and Fu (2007) found that the scattering properties are not sensitive to the aspect ratio. Figure 2 shows the aerosol backscatter ratio, ABSR, as function of aspect ratio and radius $r = (3V/4\pi)^{1/3}$. Within a range of A differing by $\pm 20\%$ from assumed aspect ratio, for a given r , the calculated ABSR may differ from the values at $A = 0.75$ by up to a factor of 2. This uncertainty needs to be taken into account when interpreting the sonde measurements.

4 Results

A total of more than 500 nights were analyzed during a 2.5 yr period with respect to the suitability to perform match flights. Of these 500 nights about 30 satisfied the match criteria between Payerne and the greater area of Zurich. Even though there were more

Balloon-borne match measurements

A. Cirisan et al.

Title Page

Abstract

Introduction

Conclusions

References

Tables

Figures

◀

▶

◀

▶

Back

Close

Full Screen / Esc

Printer-friendly Version

Interactive Discussion



days with a favourable match situation, other factors dominated the decisions not to perform the launches, such as ground weather conditions, limited human resources on either site, lacking COSMO-2 forecasts for the scheduled day etc. During 9 of these 30 nights match flights have actually been performed (e.g. because the weather situation became favourable only briefly before the required flight time). Three of these 9 launches suffered from technical problems during flight caused by one of the GPS receivers or from unexpected launch problems (such as rain). Table 1 shows the dates of the nine match flights, including information about the location of the downstream sounding in the surrounding of Zurich, the closest obtained match distance and the altitude where this distance occurred. The upstream sounding was always performed from Payerne at 46.81° N latitude and 6.94° E longitude. Match values are based on balloon GPS data and trajectories from NWP analysis data. GPS/analysis-based match distances show finite values of a few kilometres (whereas the best distance in a forecast is zero by definition). In what follows we present the match flight case with the best match distance performed on 8 June 2010.

4.1 Match forecast and analysis

The latest available COSMO-2 forecast from 15 UTC on 8 June 2010 confirmed favourable match situation as suggested by ECMWF and COSMO-7 forecasts a few days earlier. Air was approaching Switzerland from the Atlantic Ocean, west of Portugal, in a flow with relatively small horizontal wind shear, and above 8.5 km also small vertical wind shear (Fig. 3a). The air was moist but cloud-free over the Atlantic, and was forecast to cool, thus resulting in conditions for cirrus formation when approaching Switzerland. The time for the first sounding from Payerne was set, and then the time and location of the second sounding was determined by choosing the best match trajectory that fulfilled the criteria outlined in Sect. 2.

The sounding from Payerne was scheduled for 20:00 UTC, but realised 4 min later, while the one in the surrounding of Zurich from [47.45° N, 7.85° E] started exactly at 21:28 UTC as scheduled. Ground conditions were dry at Payerne, but with episodic,

Balloon-borne match measurements

A. Cirisan et al.

[Title Page](#)[Abstract](#)[Introduction](#)[Conclusions](#)[References](#)[Tables](#)[Figures](#)[◀](#)[▶](#)[◀](#)[▶](#)[Back](#)[Close](#)[Full Screen / Esc](#)[Printer-friendly Version](#)[Interactive Discussion](#)

very light drizzling rain at the upstream position, which almost put the launch at stake. The location of the second sounding is presented as a red point in Fig. 3b. The colored curves show the spread in air parcel trajectories for different altitude levels based on the COSMO-2 analysis data starting from the Payerne GPS track, indicating that the trajectory at 9.4 km yields the best match distance with the second balloon launch. The analysis data reveal a relatively small but significant horizontal wind shear, pointing to the highly dynamical processes in the atmosphere, that compromises the column box model approach. The forecast predicted significantly less wind shear than the analysis revealed, namely an angular spread only about half as large as that shown in Fig. 3b. Furthermore, given horizontal wind velocities of ≈ 70 km/h in 6 km - 12 km altitude range, the delay of 4 minutes in the upstream launch can already be responsible for a few kilometres of mismatch.

In order to validate the match accuracy and the quality of the NWP forecast, the air parcels initialized from the GPS balloon track in Payerne and followed by COSMO-2 analysis trajectories are related to the GPS balloon track from the Zurich sounding. Thus the match distances calculated from the forecast and from the analysis are compared. As mentioned before, the simultaneous shortest distance between the air parcel trajectory initialized from the Payerne GPS balloon track and the Zurich balloon GPS recording is calculated on isentropic surfaces for each level. Figure 4 shows these match distances as a function of altitude for COSMO-2 forecast and analysis fields. In the forecast case the smallest match distance between the forecast trajectories and the balloon track is at 9.0 km altitude, while it is at 9.3 km when using the analysis wind fields. In reality, when replacing the balloon simulation by the GPS balloon tracks, the closest approach to the COSMO-2 analysis trajectories is at 9.4 km altitude with a distance of 1.7 km. This confirms that the forecasting tool is successful in matching the target air parcel with a distance better than a few kilometres.

4.2 Observations

Figure 5 shows the radiosonde profiles for the night of 8 June 2010. COBALD measurements are presented by the backscatter ratios at 870 nm wavelength (red curve), while cyan and magenta show the relative humidity with respect to ice assuming solid condensate on the SnowWhite mirror and relative humidity with respect to liquid, respectively. The thin dashed dark and light blue lines in Fig. 5 indicate the RH_{ice} and RH_{liq} as measured by the Humicap sensor. As expected, the Humicap provides very good RH_{ice} up to about 6 or 7 km altitude, but becomes too slow to follow the moisture structure at higher levels, as is strikingly clear from the sudden drop in humidity at the tropopause captured well by the SnowWhite. Subsequently we will not make use of the Humicap data. The error analysis for COBALD limits its uncertainty to ± 8 – 10% of backscatter ratio at 870 nm. For SnowWhite, the nominal uncertainty is $\pm 3\%$. However, as we will see below, the accuracy in one of the measurements has most likely been severely compromised leading to a systematic error of likely rather 20–30%.

The BSR approaches values close to unity (molecular Rayleigh backscatter) in layers with very low aerosol concentrations, i.e. around 4.5 km altitude and in the lower stratosphere. Conversely, there is a thick cloud layer above both sites between 6 and 13 km, with particle sizes larger than $3\ \mu\text{m}$ indicated by the CI (not shown here). The humidity and temperature measurements suggest that the observed thick cloud consisted of a mixed-phase cloud below 7.5 km altitude and a cirrus cloud above, which we will show to be consistent with box model simulations. Between 3 and 4 km another broad peak in BSR points to the presence of mist, containing swollen aerosols. Interestingly, the Zurich sonde reveals a pronounced boundary layer inversion of 3–4 °C. At the ground the air was very moist with $RH_{liq} \sim 100\%$, i.e. at the onset of rain. Some of the problems with this sounding discussed below might be related to raindrops that might have collided with the housing of the SnowWhite sensor. This is different at Payerne with $RH_{liq} \sim 95\%$.

Title Page

Abstract

Introduction

Conclusions

References

Tables

Figures

◀

▶

◀

▶

Back

Close

Full Screen / Esc

Printer-friendly Version

Interactive Discussion



The Payerne sounding shows a gap in backscatter between 9 and 10 km resulting in two separate cirrus layers, but when the air arrived over Zurich, the gap was filled. There are several possible explanations:

- (a) the gap might have been filled by ice crystals sedimenting from higher levels;
- (b) it might have been filled by new particle nucleation;
- (c) or due the presence of internal dynamics and instabilities (shallow convection) within the cloud;
- (d) or wind shear might have led to different air masses being transported into the gap layer.

Hypotheses (c) and (d) cannot be investigated by a trajectory column approach. In particular we have no means to rule out (d), apart from the fact that the cloud gap and its filling is observed exactly at the best match altitude rendering wind shear effects a questionable explanation. Hypothesis (c) may be investigated by inspection of stability along the two balloon tracks. Equivalent potential temperature is a good indicator for potentially unstable layers in an air column (Houze, 1993), which takes temperature changes in an air parcel resulting from potential latent heat release or consumption upon cloud particle condensation/evaporation into account. It is defined as $\theta_{\text{eq}} = \theta \exp(L_s q_v / c_p T)$, where L_s denotes the latent heat of sublimation, q_v the mixing ratio of water vapour mass per mass of dry air, c_p the specific heat of dry air at constant pressure and $\theta = T \times (\rho_0 / p)^{2/7}$ is the potential temperature with air temperature T and pressure at the earth surface ρ_0 . The stability criterion reads

$$\frac{\partial \theta_{\text{eq}}}{\partial z} \begin{cases} > 0, \text{ potentially stable} \\ = 0, \text{ potentially neutral} \\ < 0, \text{ potentially unstable} \end{cases} \quad (2)$$

Figure 6 shows the equivalent potential temperature θ_{eq} derived from p , T and q_v for both soundings. While a potential instability is present between 6.5 km and 8 km

Balloon-borne match measurements

A. Cirisan et al.

Title Page	
Abstract	Introduction
Conclusions	References
Tables	Figures
◀	▶
◀	▶
Back	Close
Full Screen / Esc	
Printer-friendly Version	
Interactive Discussion	



Balloon-borne match measurements

A. Cirisan et al.

Title Page

Abstract

Introduction

Conclusions

References

Tables

Figures

◀

▶

◀

▶

Back

Close

Full Screen / Esc

Printer-friendly Version

Interactive Discussion



over Payerne in the altitude layer supporting the supercooled liquid cloud, at cirrus levels the atmosphere is potentially stable or neutral. The same holds for the Zurich sounding, containing an unstable layer below 7 km, as well as a shallow layer around 11 km, which might potentially be unstable. This instability might indicate the presence of shallow convection inside cirrus clouds, as proposed and investigated by Spichtinger (2013). Overall, the Zurich profile suggests more dynamical activity on 100–200 m altitude scales, which may lead to vertical air mass exchange over this altitude range, but none of the profiles suggests convection to an extent that would prohibit a trajectory analysis.

Explanations (a) and (b) are investigated in the subsequent sections first by detailed comparison with COSMO data, then by comprehensive microphysical modeling, and finally by a discussion of the quality of the RH_{ice} data. Concerning the closure of the cloud gap between 9 and 10 km altitude, as we will see below, the model provides evidence against extensive ice particle sedimentation (explanation (a)), but clearly supports new ice nucleation between Payerne and Zurich (explanation (b)).

4.3 Comparison of COSMO-7 fields with measurements

We intend to investigate the microphysical changes in the air mass travelling from Payerne towards the second launch location using a spectral (i.e., particle size resolving) column box model, driven by temperature and pressure fields from COSMO-7 analysis (the COSMO-2 domain is too small for this purpose). The trajectories have been calculated forward and backward from the flight track of the balloon launched from MeteoSwiss station at Payerne, covering the altitude range of 5 to 12.6 km with 100 m vertical intervals. The starting point for the initialization of the box model was chosen 16 h upstream the Payerne sounding, beginning the simulation with cloud-free conditions in all trajectory levels. This avoids having to initialize the ice distribution, which cannot be extracted from the measurements.

Prior to the comprehensive microphysical modeling, we validate the accuracy of COSMO-7 analysis fields comparing temperature, humidity, ice and vapour mixing ra-

Balloon-borne match measurements

A. Cirisan et al.

Title Page

Abstract

Introduction

Conclusions

References

Tables

Figures

◀

▶

◀

▶

Back

Close

Full Screen / Esc

Printer-friendly Version

Interactive Discussion



5 tio profiles extracted along the balloon tracks with the measured data. As we will see below, COSMO-7 misjudges the phase of the warming by about half hour, i.e. COSMO runs early. We therefore compared the observed and modeled data not only at the position of the balloon (green curves in Fig. 7), but also for a position half hour up-

10 stream (black curves in Fig. 7). The temperature difference between the model value and measurement is presented in panels a and e of Fig. 7 for Payerne and Zurich, respectively. The altitude range of interest is between 400 hPa and 180 hPa. COSMO temperatures are in excellent agreement with the Payerne sonde, but are ~ 2 K warmer than the temperature measured by the Zurich sonde between 250 hPa and 200 hPa.

15 This is exactly where the upper part of the measured cirrus cloud was located. Water vapour mixing ratios of the model relative to the measurement over Zurich (Fig. 7f) appear 20 % lower, which is also reflected in the RH_{ice} profile (Fig. 7g), whose upper part of the cloud is subsaturated in the model by almost 30 %. Correspondingly, the COSMO IWC (Fig. 7h) indicates no presence of an ice cloud at these altitudes, i.e. the trajectories are too warm and too dry at the time they reach the Zurich region. This makes them bad candidates for driving the microphysical model in order to produce the measured high supersaturations. Another NWP caveat potentially contributing to the erroneous humidity representation is the one-moment bulk microphysics scheme implemented in COSMO, which is not able to capture the fine measured structure and prevents the persistence of ice supersaturation. Following a similar procedure as in Brabec et al. (2012) we compare COSMO IWC to the IWC estimated from the BSR measurements. To this end we assume the ice crystal mode radius r_m of in-situ formed cirrus clouds to lie in a typical range of $5 \mu\text{m}$ to $20 \mu\text{m}$, yielding an overall uncertainty in the BSR of a factor of ~ 4 . Over Payerne, the COSMO data suggest the existence of a single cloud layer with a maximum in IWC exactly where the gap between the two cloud layers is detected by the measurements (Fig. 7d). Over Zurich the lower part of the cloud is represented by COSMO data, overestimating IWC values by one order of magnitude as compared to the measured values, while the uppermost part of the cloud is completely missed.

20

25

Balloon-borne match measurements

A. Cirisan et al.

Title Page

Abstract

Introduction

Conclusions

References

Tables

Figures

◀

▶

◀

▶

Back

Close

Full Screen / Esc

Printer-friendly Version

Interactive Discussion



the Pyrenees are apparent in the increased trajectory wave activity around 10:00–12:00 UTC. The region between Payerne and Zurich is indicated by the balloon tracks as green lines in Fig. 8. This region is particularly interesting, because it marks the end of the overall cooling, showing some significant warming at altitudes above 9 km, leading to a partial evaporation of the high clouds. Therefore, the measurements from Zurich took place in a situation with evaporating clouds, and a small error by COSMO-7 in the phase of the warming renders the presentation of the observed clouds difficult.

Figure 9 shows model simulations for relative humidity with respect to ice (RH_{ice}), ice crystal number density (n_{ice}), ice mixing ratio (defined as number density of water molecules condensed in ice divided by the number density of air molecules) and aerosol backscatter ratio (BSR at 870 nm) calculated by the ZOMM microphysical column model driven by winds, pressures and temperatures from COSMO-7 analysis fields. In the model, shortly after 7 UTC the first cloud is forming around 330 hPa in ascending air masses above the Pyrenees. This cloud is at relatively low altitudes ($H < 8$ km) and high temperatures ($T > 245$ K), clearly warmer than the homogeneous ice nucleation threshold of 235 K (Koop et al., 2000) and thus represented in the model as a supercooled liquid cloud with a very strong backscatter (red color, Fig. 9d). We emphasize that the modeled numerical value of the backscatter ratio of this liquid cloud is unrealistically high (BSR ~ 1000), because ZOMM, though containing all relevant processes for cold cirrus clouds, does not describe processes in warmer mixed phase clouds (coagulation and heterogeneous nucleation in liquid clouds are not implemented).

At about 10:00 UTC, the model forms the first ice cloud in a thick layer between 230 and 280 hPa ($H \sim 9$ –10 km). Ice crystal number densities in Fig. 9b remain low (mostly $n_{ice} \leq 0.1 \text{ cm}^{-3}$), and almost vertical fall streaks to altitudes below the previous supercooled water cloud originate from large, quickly sedimenting ice particles. Forced by continuous upwelling all the way to Payerne, the model forms a succession of ice clouds at various altitudes ($H \sim 9$ –13 km), which quickly sediment and/or sublimate, as well as persistent supercooled liquid clouds at $H \sim 6$ –9 km.

Balloon-borne match measurements

A. Cirisan et al.

Title Page

Abstract

Introduction

Conclusions

References

Tables

Figures

◀

▶

◀

▶

Back

Close

Full Screen / Esc

Printer-friendly Version

Interactive Discussion



As mentioned above, there is a pronounced warming phase between Payerne and Zurich. In the model, this leads to subsaturated conditions with $RH_{ice} \sim 75\%$ in the vicinity of the Zurich sounding (Fig. 9a). This causes an immediate suppression of further cloud formation and gravitational removal or sublimation of remaining ice particles until no ice is left (Fig. 9c). Only a thick supercooled liquid cloud at lower levels survives, and Meteosat cloud images confirm that the air masses completely clear up further downstream, with a sunny morning over large parts of Switzerland and south-east Germany.

Figure 10 shows the resulting profiles of BSR and RH_{ice} , comparing measured and calculated values (panels a, b, e, f) not only at the position of the balloon (green curves) but also with a position half hour upstream (black curves). Since $RH_{ice} = \chi_w p / p_{ice}(T)$ is a function of both, the local temperature (via the ice vapour pressure $p_{ice}(T)$) and the local water mixing ratio (via the water partial pressure $\chi_w p$), we also compare measured and modeled temperatures (i.e. $T_{mod} - T_{meas}$, panels d and h) and the relative water mixing ratio (i.e. $(\chi_{w\ mod} - \chi_{w\ mod} - \chi_{w\ meas}) / \chi_{w\ meas}$, panels c and g). The comparison with the Payerne sounding shows that the model manages to capture the clouds below 11 km very well, but misses the clouds between ~ 11 km and the tropopause at 12.6 km altitude (Fig. 10a). Because $RH_{ice} > 100\%$ in the model, this deficiency must be due to a too fast gravitational removal, i.e. too large ice particles. The comparison with the Zurich sounding discloses a complete failure of the model, which has lost all ice clouds (Fig. 10e). In the altitude range 8–12.6 km (180–350 hPa) the COSMO temperatures are too warm by more than 2 K (Fig. 10h, green curve), indicating the phase error in the onset of the warming. This improves by displacing the temperatures upstream by 30 minutes (black curves), reducing the difference in RH_{ice} , but does not establish the supersaturation observed by the Zurich sonde (Fig. 10f, blue curve). Yet, even with the displacement the cirrus clouds above Zurich cannot be fully established (Fig. 10e).

In summary, ZOMM manages to capture very well both, BSR and RH_{ice} measured by the Payerne sonde, except for the highest cirrus between 11 km and the tropopause at 12.6 km. Conversely, the model fails to reproduce the measurements by the Zurich

sounding about 1.5 h downstream. This failure is partly due to a COSMO phase error, but even when this is corrected, ZOMM forced by the original COSMO meteorological fields cannot reproduce the observed supersaturation in a thick cirrus layer at 10-12 km altitude.

5 4.5 Small-scale temperature fluctuations and other unknowns

One known important reason for the model's inability to represent the more persistent cirrus layer in the upper part of the profile is its lack of small-scale temperature fluctuations, i.e. unresolved variations along the air mass trajectories, which affect cooling rates and therefore cause mostly higher ice crystal number densities, smaller radii, smaller sedimentation speeds and longer cirrus life time. Other unknowns are certain microphysical properties, e.g. of the mass accommodation coefficients, which may delay the sublimation of ice, or the presence of heterogeneous ice nucleation on a few pre-existing ice nuclei. In what follows we use the match experiment data to discuss these model aspects.

15 4.5.1 Small-scale temperature fluctuations

In order to reproduce the unresolved small-scale temperature fluctuations ($(dT/dt)_{ss}$), characteristic fluctuations were superimposed on the trajectories derived from the COSMO-7 meteorological data. We refine a procedure that has been used for a similar purpose by Brabec et al. (2012). The fluctuation frequency spectrum was adopted again from Hoyle et al. (2005) based on the vertical wind and temperature measurements from the "Subsonic Aircraft: Contrail and Cloud Effects Special Study" (SUCCESS) campaign. The $(dT/dt)_{ss}$ applied here were constructed from the SUCCESS data such that only wavelengths smaller than 30 km are retained. This cut-off wavelength is chosen because longer wavelength perturbations are already resolved by the 7 km grid spacing of COSMO-7. Concerning the proper choice of fluctuation amplitudes, three different scenarios were analyzed: clear sky, cloudy sky and – as a

combination of both – “all sky” conditions. This approach basically assumes a quasi-universal form of the spectral shape of gravity wave motions, whose amplitude can be scaled to reflect space and time differences. This is largely supported by considerable research activity in this area over the past two decades (Fritts and Alexander, 2003).

For the fluctuation amplitudes we use the work by Gallice et al. (2011), who showed that information on air vertical motion can be derived from the ascent rate of sounding balloons. The deviation of the observed ascent of a sounding balloon from the one expected in vertically quiet air, as derived from a detailed treatment of the balloon motion taking internal heat flow and skin friction into account, is caused by the vertical motion of the air. Much simplified, but agreeing in general with this work, the vertical wind of air (w) can be estimated from the original ascent data of the sounding balloons by subtracting a 500-s running mean (boxcar over 500 one-second GPS measurements), which represents approximately the ascent of the balloon in quiet air.

The $(dT/dt)_{ss}$ can be readily calculated from w : $(dT/dt)_{ss} = -(dT/dz) \times w$, where dT/dz is the adiabatic lapse rate (~ 10 K/km). The average cooling rate outside of clouds was determined from the GPS data recorded during 10 radiosonde ascents performed from Payerne and Zurich during the last years. An average cooling rate of $\langle (dT/dt)_{ss} \rangle_{clear} = -12$ K h⁻¹ was obtained from these soundings (where $\langle \dots \rangle$ is the arithmetic mean taken over all negative rates), comparing well with the mean -11 K h⁻¹ found in convectively unperturbed periods during SUCCESS (Hoyle et al., 2005). The average cooling rate in clouds extracted from the present two flights exhibits almost twice the cooling rate of the clear sky scenario, $\langle (dT/dt)_{ss} \rangle_{cloudy} = -23$ K h⁻¹, which we attribute to small-scale cloud internal dynamics. Using the average clear and cloudy sky fluctuations, we scale the SUCCESS data by adjusting the fluctuation amplitudes from Hoyle et al. (2005), and from this obtain a mean fluctuation amplitude. The “all sky” scenario superimposes cloudy sky T -fluctuations on those parts of the trajectories, where ZOMM determined clouds, and clear sky T -fluctuations on cloud-free parts. As criterion to distinguish between these cases we use the ice number density threshold $n_{ice} > 10$ L⁻¹ within ZOMM. In addition we require $RH_{ice} < 1.35$ as indicator for the end

Balloon-borne match measurements

A. Cirisan et al.

Title Page

Abstract

Introduction

Conclusions

References

Tables

Figures

◀

▶

◀

▶

Back

Close

Full Screen / Esc

Printer-friendly Version

Interactive Discussion



of the homogeneous nucleation event and beginning of the cloudy phase with release of latent heat and subsequent small-scale turbulence.

Each of these three sets of small-scale fluctuation distributions was used as basis for an independent, comprehensive column model calculation in order to demonstrate the consequences of the fluctuations on the cirrus cloud properties. For each set ten randomly chosen fluctuation sequences (such as those shown by Hoyle et al. (2005) in their Fig. 2) were superimposed onto the COSMO trajectories. As a generic result, the application of any of the three fluctuations sets improves the agreement with the sonde measurements significantly by letting the clouds develop less pronounced fall streaks and survive to the Zurich sounding and beyond, with n_{ice} enhanced by more than one order of magnitude compared to the scenario without fluctuations. Figures 11 and 12 show an example applying the fluctuations of the “all sky” scenario. Differences in the impact of clear, cloudy and “all sky” fluctuations on cirrus properties are much smaller than the difference between the scenario without fluctuations (Fig. 9 and 10) compared to any of the fluctuation scenarios discussed here.

As a metric to objectify the quality of the match between the model results and the measurements we introduce the quantity

$$M = \int_{9 \text{ km}}^{12.5 \text{ km}} dz \ln \text{BSR}_{\text{mod}} / \int_{9 \text{ km}}^{12.5 \text{ km}} dz \ln \text{BSR}_{\text{meas}} - 1 \quad (3)$$

This metric uses the backscatter ratio, because it integrates all cloud processes over a wide range of meteorological conditions upstream of the measurement. It is therefore largely independent of the instantaneous temperature fluctuation at the location and time of the measurement. In contrast, relative humidity depends strongly on the temperature in the moment of the measurement and, hence, is not considered to be suited to judge the quality of the cloud modeling. The logarithmic form of Eq. (3) ensures that not only the largest BSR enter the evaluation.

Balloon-borne match measurements

A. Cirisan et al.

Title Page

Abstract

Introduction

Conclusions

References

Tables

Figures

I◀

▶I

◀

▶

Back

Close

Full Screen / Esc

Printer-friendly Version

Interactive Discussion



Balloon-borne match measurements

A. Cirisan et al.

Title Page

Abstract

Introduction

Conclusions

References

Tables

Figures

◀

▶

◀

▶

Back

Close

Full Screen / Esc

Printer-friendly Version

Interactive Discussion



Graphically, Eq. (3) is the relative area between the model curves and the measurements in Fig. 10a,e or 12a,e (with a lower limit taken at the upper edge of the liquid cloud). The metric accounts only for deviations in mean values, not for the mean squared error, in order to exclude altitude errors, which would be likely more an error of the underlying meteorological model than of the microphysical treatment. Therefore, in Fig. 12a, the cloud gap above Payerne is modeled at an altitude too low by about one kilometre, and the metric does not punish this fact.

Table 2 lists the results for M (in %) for the scenario without fluctuations and with superimposed clear, cloudy and “all sky” fluctuations. In order to obtain the information in Table 2 M was calculated independently for each of the 10 fluctuation runs in each scenario, and the run agreeing best with the Payerne and Zurich measurements is listed (evaluated at the half hour upstream position). The scatter in M between different fluctuations is substantial: for example, the scenario for clear sky conditions at Payerne with $M = -15\%$ may for other fluctuations be as bad as $M = -62\%$. Once again, this illustrates the sensitivity of the cloud results to fluctuation events that might have happened far upstream.

Clearly, the major improvement over the scenario using the COSMO trajectories only (left column in Table 2) is the introduction of fluctuations, while the differences between the particular type of fluctuations are less important. Here, the parameterization using the cloudy sky conditions yields the best agreement with the observations. However, we will see below that microphysical uncertainties are in the same range as the differences between the various fluctuation scenarios. Therefore, different microphysical assumptions may make other fluctuation scenarios more favorable.

There is an ambiguity as how to superimpose the $(dT/dt)_{ss}$ fluctuations onto the COSMO-based trajectories concerning their phase relation within the air column. The two extremes are either a completely random application, i.e. each trajectory has a different sequence of $(dT/dt)_{ss}$, or fluctuations are in phase for all altitudes. The real atmosphere is somewhere in between. In this work we apply fluctuations in phase for all altitudes. We will return to this question in Sect. 4.5.4.

Balloon-borne match measurements

A. Cirisan et al.

Title Page

Abstract

Introduction

Conclusions

References

Tables

Figures

◀

▶

◀

▶

Back

Close

Full Screen / Esc

Printer-friendly Version

Interactive Discussion



In passing we note that we also investigated the impact of latent heat release on the trajectory temperatures, which might differ between the microphysics schemes in COSMO and in ZOMM. We performed full ZOMM column calculations based either on the diabatic COSMO 3D trajectories (which include latent heat and radiative effects), or on adiabatic trajectories using only the COSMO pressure as input and correcting for the latent heat release within ZOMM itself. Results are slightly better with the adiabatic trajectory approach, but the differences are not significant. Figure 11 and subsequent figures therefore show results from the adiabatic approach.

Figure 12 shows the comparison between the measured BSR and RH_{ice} over Zurich and Payerne and the profiles taken from Fig. 11 at the 30 minute upstream position (i.e. black balloon track in Fig. 11). Black lines in Fig. 12 show the single model member with the fluctuations that agree best with the observation in terms of M (i.e., the computation using same member, Fluctuation No. 6, evaluated at both positions), while the grey shaded area shows the results for all 10 ensemble members with the randomly chosen fluctuations.

Comparing the BSR profiles at both locations we conclude that the cloud gap around 320 hPa is filled up on the way between Payerne and Zurich, either due to formation of new particles or by sedimentation from the levels above, with modelled BSR and number densities of the ice crystals increasing by about one order of magnitude. This cloud gap above Payerne is also clearly visible in all panels of Fig. 11, which basically verifies the quality of the COSMO-7 temperature fields enabling ZOMM to model this gap. The model succeeds in filling this cloud gap (compare black curves in Fig. 12a and Fig. 12e). From Fig. 11a it is clear that between Payerne and Zurich the air cooled to reach conditions of homogeneous nucleation, and the stepwise increase in n_{ice} and BSR in Fig. 11b, d shows that the gap was filled by a new nucleation event in the midst of clouds. However, from the grey ensemble area in Fig. 12e it is also clear that not each ensemble member is doing this job, i.e. the exact choice of ensemble member plays a big role in achieving agreement with the measurement. This highlights once again the importance of small-scale temperature fluctuations (dT/dt)_{ss} and our limited ability

to provide a deterministic picture. Rather, we have to rely on probabilistic analyses, similar to weather forecasts where weather services have also begun to make full use of ensemble member analysis.

4.5.2 Mass accommodation of H₂O on ice

5 Aside from meteorological processes on the small scale (e.g. $(dT/dt)_{ss}$), which force the microphysics of cirrus, there are other independent microphysical aspects, which affect cirrus properties. At low temperatures clean ice is thought not to develop a quasi-liquid surface layer, but the water molecules rather need to be accommodated directly on the crystalline ice surface. Accommodation is impeded, even when RH_{ice}
10 $> 100\%$, because molecules need to arrive at a suitable position on the surface and in the right orientation, or else will be either reflected back into the gas phase or adsorbed only loosely and subject to rapid desorption. This impedance has been ascribed to conditions when the outermost lattice monolayer is complete and a new monolayer needs to start via “surface nucleation”. In analogy, H₂O molecules do not evaporate
15 at $RH_{ice} < 100\%$ without impedance: when the outermost lattice monolayer has completely evaporated, defects need to “nucleate” first in order to facilitate further evaporation. These processes are traditionally quantified by a mass accommodation coefficient ($\alpha \leq 1$), which comprises all details of the surface processes and describes the probability of H₂O molecules condensing to/evaporating from an ice surface compared with
20 the absence of the surface impedance. Surface impedance has been discussed as a potential mechanism to explain high and persistent in-cloud supersaturations (Peter et al., 2006, 2008). The similarity of these processes with nucleation explains why α is likely a function of supersaturation, i.e. $\alpha = f(RH_{ice})$, see e.g. MacKenzie and Haynes (1992) or Wood et al. (2001).

25 The literature reports a broad range of values for the mass accommodation coefficient of water on ice (Stephens, 1983; Lin et al., 2002; Gierens et al., 2003; Magee et al., 2006). The surface nucleation rate depends critically on local saturation in the vicinity of the ice surface. For large ice particles and small gas phase saturation, α

Balloon-borne match measurements

A. Cirisan et al.

Title Page

Abstract

Introduction

Conclusions

References

Tables

Figures

◀

▶

◀

▶

Back

Close

Full Screen / Esc

Printer-friendly Version

Interactive Discussion



can be smaller than 0.01, while for small ice particles and high gas phase saturation it approaches unity. ZOMM describes this in a simplified way relating α to the water saturation ratio directly over the ice surface $S = p_w^{\text{surf}}/4p_w^{\text{ice}}$: for small $|S - 1|$ growth/evaporation relies on the existence of defects (dislocations) on the ice surface, which lead to a continuous uptake (i.e. a constant accommodation coefficient α_0); for large $|S - 1|$, growth/evaporation proceeds by two-dimensional nucleation of new stable nuclei on the ice surface. This is modeled by classical nucleation theory: the Gibbs energy of 2D-disk of a monolayer with radius r on the ice surface is given by

$$G = \frac{\pi r^2}{A_1} kT \ln S + 2\pi r \Gamma, \quad (4)$$

where A_1 is a cross section of H_2O molecules, k is Boltzmann constant, T is temperature, S is the saturation ratio microscopically above the ice surface, which may deviate from the ambient relative humidity RH_{ice} (see below), and Γ is the step energy per unit length.

The formation energy of the 2-D-disk with critical size r , G_f , can be obtained from $dG/dr = 0$, resulting in

$$G_f = \frac{\pi A_1 \Gamma^2}{kT \ln S}. \quad (5)$$

The saturation ratio microscopically above the ice surface S can be derived from considerations regarding the H_2O molecule flux to/from the ice particle. When N_w is the number of H_2O molecules diffusing to an ice crystal with radius a , this flux can be either described by the gas phase diffusion equation (Pruppacher and Klett, 1997)

$$\frac{dN_w}{dt} = 4\pi a \frac{D_w}{1 + \frac{4D_w}{\alpha av}} n_{\text{vap}} (\text{RH}_{\text{ice}} - 1), \quad (6)$$

which takes account of the diffusion impedance in the gas volume, or by the Knudson diffusion

$$\frac{dN_w}{dt} = 4\pi a^2 \frac{\alpha \nu n_{\text{vap}}(S-1)}{4}, \quad (7)$$

which accounts for the surface impedance related to mass accommodation. Here, D_w is the gas phase diffusion coefficient of water molecules in air, α is the mass accommodation coefficient of H₂O on ice surface, ν the thermal mean velocity of water molecules, and n_{vap} is the equilibrium H₂O vapor concentration over ice surface.

From equating Eqs. (6) and (7), the saturation ratio above the ice surface S is given by

$$S = (1 + bRH_{\text{ice}}) / (1 + b), \quad (8)$$

where $b = 4D_w / (\alpha \nu)$ describes the reduction of the super- or subsaturation from far away to the particle surface due to gas diffusive volume impedance. Equation (8) describes the reduction of $|RH_{\text{ice}} - 1|$ to $|S - 1|$ due to the impedance on ice surface by gas phase diffusion.

The nucleation rate coefficient is then calculated as

$$j = \frac{kT}{h} \exp\left[-\frac{\Delta F_{\text{diff}}(T)}{kT}\right] \times n_w \exp\left[-\frac{\Delta G_f(T)}{kT}\right], \quad (9)$$

where F_{diff} is the diffusion activation energy on the surface and n_w is the area number density of water molecules on an ice surface.

Finally, the number of surface layers nucleating within a time interval by surface nucleation depends on the surface area of the crystal plane, $A (=a^2)$, the time required to fill the layer via gas phase diffusion, τ_{ml} , and the nucleation rate coefficient, j . From this the mass accommodation coefficient is approximated by the following equation

$$\alpha = 1 - \exp(-Aj\tau_{\text{ml}} - \alpha_0), \quad (10)$$

Balloon-borne match measurements

A. Cirisan et al.

Title Page

Abstract

Introduction

Conclusions

References

Tables

Figures

◀

▶

◀

▶

Back

Close

Full Screen / Esc

Printer-friendly Version

Interactive Discussion



which exhibits the correct limits ($\alpha \rightarrow \alpha_0$ for very small particles or small $|\text{RH}_{\text{ice}} - 1|$, and $\alpha \rightarrow 1$ for very large A or large $|\text{RH}_{\text{ice}} - 1|$). The above treatment of monolayer nucleation leaves Γ , the step energy per unit length, and α_0 , the minimum mass accommodation coefficient, as the only unknowns. These are determined by fitting to data of laboratory experiments. Here we use the ice particle growth measurements for the cirrus regime performed by Magee et al. (2006), because they determined particularly low accommodations with $\alpha < 0.01$. With this choice, maximum effects on the calculated cirrus cloud properties are expected. The resulting dependence of α on the ambient relative humidity RH_{ice} is depicted in Fig. 13, showing that larger particle sizes have indeed smaller α in the nucleation regime. As the ice crystals grow to larger sizes, α decreases because the gas diffusion impedance diminishes the super- or subsaturation directly above the crystal surface, $|S - 1|$, in comparison to the ambient $|\text{RH}_{\text{ice}} - 1|$.

Despite the fact that our approach here assumes α to deviate considerably from values around unity, the consequences for the modeled BSR of the Payerne and Zurich soundings are moderate, as the results in Table 3 show. The calculations for Table 3 are similar to Table 2, just replacing $\alpha = 1$ by $\alpha = f(\text{RH})$. Compared to Table 2, the reduction in α leads to reduced sensitivity of the ice particles against evaporation in the warming phase and thus to a general increase of BSR, and thus M in Table 3. The “all sky” scenario listed in Table 3 is identical to Fig. 12a, e.

4.5.3 Heterogeneous nucleation of ice

We finally investigated how the existence of a small number of heterogeneous ice nuclei influences the cirrus formation, and whether the expected effects improve the model-measurement agreement. ZOMM has been used previously for heterogeneous ice nucleation in the immersion mode, see Engel et al. (2013), and we closely follow their treatment. From classical nucleation theory (Pruppacher and Klett, 1997), the heterogeneous rate coefficient J_{het} for ice nucleation (units of $\text{cm}^{-2} \text{s}^{-1}$) is formulated

as

$$j_{\text{het}}(T) = \frac{kT}{h} \exp\left[-\frac{\Delta F_{\text{diff}}(T)}{kT}\right] \times n_w \exp\left[-\frac{\Delta G_f(T)f_{\text{het}}}{kT}\right] \quad (11)$$

where k is the Boltzmann and h the Planck constant, and n_w is the number density of water molecules at the interface between water and the ice nucleus (taken as 10^{15} cm^{-2}). The diffusion activation energy ΔF_{diff} and the Gibbs free energy ΔG_f are parameterized according to Zobrist et al. (2007) and references therein. The ice saturation ratio S in the liquid enters into the calculation of ΔG_f and is defined for immersion freezing as $S = p_w^{\text{liq}}(T) / p_w^{\text{ice}}(T)$. Vapour pressures of liquid water and ice are calculated following Murphy and Koop (2005). The compatibility function, $F_{\text{het}} < 1$, discriminates homogeneous and heterogeneous nucleation, as it describes the reduction of the energy barrier ΔG_f , which needs to be overcome to form a critical ice embryo:

$$f_{\text{het}} = \frac{1}{4}(2 + \cos \gamma)(1 - \cos \gamma)^2 \quad (12)$$

The contact angle γ between the ice embryo and the ice nucleus can vary from 0° to 180° , which for small contact angles results in nucleation starting as soon as the vapour is saturated, whereas for large contact angles heterogeneous nucleation is not much favoured over homogeneous nucleation. Similar to Engel et al. (2013) we will utilize a parameterization for ice nucleation on mineral dust (Arizona Test Dust, ATD) obtained by Marcolli et al. (2007) from freezing experiments. They observed heterogeneous nucleation over a broad temperature range, and concluded that the ability to nucleate ice varies between different ATD particles, leading to the following “active sites” occurrence probability:

$$P_{\text{as}} = 10^{-5} \text{deg}^{-1} \times \exp\left(\frac{-51^\circ}{\gamma - 46^\circ}\right). \quad (13)$$

Active sites are surface inhomogeneities such as steps or cavities, or chemical or electrical inhomogeneities, which are assumed to initiate ice nucleation (Pruppacher and

Balloon-borne match measurements

A. Cirisan et al.

Title Page

Abstract

Introduction

Conclusions

References

Tables

Figures

◀

▶

◀

▶

Back

Close

Full Screen / Esc

Printer-friendly Version

Interactive Discussion



Balloon-borne match measurements

A. Cirisan et al.

Title Page

Abstract

Introduction

Conclusions

References

Tables

Figures

◀

▶

◀

▶

Back

Close

Full Screen / Esc

Printer-friendly Version

Interactive Discussion



Klett, 1997). Following Marcolli et al. (2007), the mean area of an active site is set to $A_{as} = 10 \text{ nm}^2$. Even though a single particle may carry several active sites, the best active site with the smallest contact angle γ is dominant and this one is treated by the model. The occurrence probability of active sites decreases with decreasing γ , i.e. the better the site the rarer it is. The number density of foreign nuclei (e.g., mineral dust), containing at least one active site with a minimum contact angle γ (i.e. the number of foreign nuclei in one particular contact angle bin), is then given by

$$n_{\gamma} = \left(n_{\text{foreign}} - \sum_{\gamma'-47^{\circ}}^{\gamma-1^{\circ}} n'_{\gamma'} \right) \times P_{as}(\gamma) \times \frac{4\pi r_{\text{foreign}}^2}{A_1}, \quad (14)$$

from which we obtain an equivalent volume-based nucleation rate of

$$J_{\text{vol}}(T) = \sum_{\gamma-47^{\circ}}^{180^{\circ}} n_{\gamma} \times J_{\text{het}}(T, \gamma) \times A_1. \quad (15)$$

The only unknown in this formulation is n_{foreign} , the overall number density of heterogeneous ice nuclei. Here we adopted the canonical value of 10 L^{-1} by DeMott et al. (2003). Table 4 lists two heterogeneous scenarios in comparison with other scenarios.

4.5.4 Comparison of cirrus formation mechanisms

In the preceding subsections we summarized a number of mechanisms possibly involved in the formation and maintenance of the cirrus clouds observed in the match flights from Payerne and Zurich on 8 June 2010:

1. homogeneous ice nucleation supported by small-scale temperature fluctuations $(dT/dt)_{\text{SS}}$,
2. impeded particle growth/evaporation, e.g. the humidity dependent mass accommodation $\alpha = f(\text{RH}) \ll 1$,

Balloon-borne match measurements

A. Cirisan et al.

Title Page

Abstract

Introduction

Conclusions

References

Tables

Figures

◀

▶

◀

▶

Back

Close

Full Screen / Esc

Printer-friendly Version

Interactive Discussion

3. heterogeneous nucleation on a few potent ice nuclei (e.g., $n_{IN} = 10 \text{ L}^{-1}$).

In addition to these major processes we also investigated the effect of using either diabatic or adiabatic trajectories (latent heat-corrected), which has a minor impact on the modeled clouds. A total of 264 column model calculations have been performed for the following scenarios: (clear or cloudy or “all sky”) \times (diabatic or adiabatic) \times ($\alpha = 1$ or $f(\text{RH})$) \times ($n_{IN} = 0$ or 10 L^{-1}) $= 3 \times 2 \times 2 \times 2 = 24$ scenarios and for each of these scenarios applying 10 random fluctuation distributions plus one without fluctuations.

In addition to comparing with the “best” fluctuation member we also calculated the median and mean values of all 10 trajectories in a scenario for each altitude (not shown). As mentioned in Sect. 4.5.1, we applied fluctuations $(dT/dt)_{SS}$ with the same phase for all altitudes. While this procedure is simple, it exaggerates the vertical dynamical coupling within an air column. We have not tried to apply a more realistic approach in our calculations, but using median or mean helps to avoid outliers at certain altitudes which, even though possible, are not very likely. The conclusions drawn from median and mean results do not differ much from the results shown in Tables 2–4, and are therefore not shown. In comparison with the single fluctuation results, median and mean results are smoother. Besides this advantage, showing the median instead of a single fluctuation case may also have drawbacks, as a comparison between the median results and second and third columns in Table 4 reveals: while the single case manages to develop the cloud gap (albeit at slightly too low altitude), the median does not. This comparison again highlights the care needed when interpreting results from an ensemble calculation: the exact nature of $(dT/dt)_{SS}$ in shaping the resulting cloud field is essential, highlighting the requirement of taking a probabilistic approach and then average, but a single member may be the best description of reality.

The synopsis of Tables 2–4 listing the metric $M = \int dz \ln \text{BSR}_{\text{mod}} / \int dz \ln \text{BSR}_{\text{meas}} - 1$ (see Eq. 3) allows to assess the ability of the various scenarios to represent the observed backscatter ratios (BSR). The major conclusions are:

Balloon-borne match measurements

A. Cirisan et al.

Title Page

Abstract

Introduction

Conclusions

References

Tables

Figures

◀

▶

◀

▶

Back

Close

Full Screen / Esc

Printer-friendly Version

Interactive Discussion



1. The introduction of small-scale temperature fluctuations $(dT/dt)_{SS}$ is the dominant factor to reach better compliance of the cloud model with the observations improving the cloud modeling beyond using trajectories directly from the regional weather forecast model COSMO-7 (compare first column of Table 2 with other columns of the same table).
2. A further moderate improvement can be achieved with additional microphysical assumptions such as assuming a surface impedance limiting the growth/evaporation of the ice particles ($\alpha = f(RH) \ll 1$, see Table 3) or the presence of heterogeneous nucleation on a few potent ice nuclei ($n_{IN} = 10 \text{ L}^{-1}$, see last two columns of Table 4). A combination of these effects did not lead to a further improvement.
3. Changes induced by the microphysical assumptions are of the same magnitude as changes induced by different assumptions for $(dT/dt)_{SS}$, e.g. when using cloudy instead “all sky” conditions (compare last two columns of Tables 2 and 3).

Moreover, introducing $\alpha = f(RH) \ll 1$ and/or heterogeneous nucleation on a few potent ice nuclei $n_{IN} = 10 \text{ L}^{-1}$ without implementing small-scale temperature fluctuations does not lead to any significant improvement in the simulation of BSR (not shown). Even though both – small α and finite n_{IN} – may lead to enhancements of RH_{ice} in the nucleation phase of the cirrus clouds, these effects are too weak to cause a significant improvement (and assuming the presence of ice nuclei leads even to a slightly larger mismatch).

These conclusions are not changed either by the uncertainty in the ice particle shape (aspect ratio), which may lead to at most a factor of 2 change in BSR (see Sect. 3.5). That the factor of 2 does not represent a large change is visually clear from Fig. 12a,e where a factor of 2 results in a minor shift of the black lines. We have recalculated Table 4 for these conditions and find the above conclusions confirmed. Specifically, for $BSR_{mod} \rightarrow 0.5 \times BSR_{mod}$ the introduction of fluctuations keeps being the leading

factor and microphysical details may possibly lead to some further improvement. For $BSR_{\text{mod}} \rightarrow 2 \times BSR_{\text{mod}}$ the introduction of fluctuations leads already to a very good agreement with the measurements, and then changes in α or η_{IN} only worsen the result.

4.5.5 Comparison of measured and modeled relative humidity

So far we have not paid much attention to the modeled RH_{ice} . As mentioned above, different from backscatter, RH_{ice} is directly sensitive to the $(dT/dt)_{\text{ss}}$ at the position of the measurement. However, it is worth noting that the model yields reasonable agreement with RH_{ice} for the Payerne sounding, see Figs. 10b and 12b, but fails to explain the supersaturation measured by the Zurich sonde, see Fig. 10f and 12f. We refrain from showing the full spectrum of the results all the other model runs because they are all similar to Figs. 12b, f. Hence, the inability of the model to reproduce the supersaturations observed above Zurich does not depend on the particular choice of fluctuation or microphysical scenario.

The supersaturation observed by the Zurich sonde is perplexing also in view of the fact that the air masses are in a general warming phase. The Meteosat cloud images confirm the evaporation of clouds, and also the COSMO-based trajectories in Fig. 8 suggest a warming by about 2 K in the upper part of the cirrus cloud, which starts about 1 h before the air arrives over Zurich. Under these circumstances a slight subsaturation is expected, but not a supersaturation.

Two explanation remain possible: either there is an unknown mechanism, e.g. a surface impedance being as high as observed by Magee et al. (2006), with mass accommodation coefficients $\alpha \leq 10^{-4}$, which hinders the water in being absorbed and bound by the ice particles present in the same volume. Laboratory experiments have shown $\alpha < 0.1$ (Pratte et al., 2006; Magee et al., 2006), which has been interpreted as colliding water molecules being trapped in a precursor state (Sadtschenko et al., 2004) on the ice surface and desorbing before being incorporated into the lattice. This inability of the surface to bind the water molecules has been related to surface disorder, which

Balloon-borne match measurements

A. Cirisan et al.

[Title Page](#)[Abstract](#)[Introduction](#)[Conclusions](#)[References](#)[Tables](#)[Figures](#)[◀](#)[▶](#)[◀](#)[▶](#)[Back](#)[Close](#)[Full Screen / Esc](#)[Printer-friendly Version](#)[Interactive Discussion](#)

Balloon-borne match measurements

A. Cirisan et al.

Title Page

Abstract

Introduction

Conclusions

References

Tables

Figures

◀

▶

◀

▶

Back

Close

Full Screen / Esc

Printer-friendly Version

Interactive Discussion



begins to develop on the topmost layers of ice at temperatures above 180 K, and thus ice surfaces are potentially disordered under all conditions prevailing atmospheric conditions. However, the effect of this surface disorder on the water accommodation is not currently known (Bartels-Rausch et al., 2012). Still, surface impedances corresponding to mass accommodation coefficients $\alpha \leq 10^{-4}$ should have been detected in the laboratory, because under such extreme conditions the uptake even by macroscopic ice surfaces ($r \sim 1$ mm) starts to display more than a doubling of characteristic uptake times. Moreover, very recently the accommodation coefficient has been reported to be > 0.1 at temperatures between 190 and 235 K (Skrotzki, 2012), which fully covers the cirrus clouds discussed here, and it is speculated whether some of the water vapour in the experiments by Magee and co-workers might possibly have deposited on the walls of the measurement cell.

In order to test the impact of very low α , we ran one case with $\alpha = 10^{-4}$. Interestingly, this run does not show any improvement in RH_{ice} over Zurich (except in the uppermost 500 m of the cloud). Reason is a subtle compensation of effects: while $\alpha = 10^{-4}$ impedes the uptake of H_2O from the gas phase, this leads to the formation of higher ice crystal number densities during phases of new particle nucleation. This, in turn, enhances the ice surface area density, which in terms of uptake kinetics largely compensates the reduced mass accommodation coefficient.

The alternative explanation is that the SnowWhite measurement of the Zurich sonde is erroneous. We consider this second explanation by far more likely. Either there could be an error in the SnowWhite frost point measurement corresponding to a water vapor mixing ratio 15–30 % too high, or the sensor measuring the ambient temperature made an error of 1–2 K (because the vapour pressure of ice changes by ~ 15 % per degree temperature change). Both the frost point mirror and the air temperature are measured using a copper-constantan thermocouple (manufactured by Meteolabor) and the measurement uncertainty (one-standard-deviation error) for the temperature sensors is ± 0.2 K according to the manufacturer. The temperature difference between the two sensors is even more precise as the sonde internal temperature reference is the same

Balloon-borne match measurements

A. Cirisan et al.

Title Page

Abstract

Introduction

Conclusions

References

Tables

Figures

◀

▶

◀

▶

Back

Close

Full Screen / Esc

Printer-friendly Version

Interactive Discussion



for both. Fortunately, there is a second independent constantan-copper thermocouple measuring temperature, with the purpose to correct the HC-2 Humicap located close to it inside the styrofoam flow channel. We compared the temperature measure by the main sensor with that of the additional sensor and found both sensors to agree within ± 0.1 K all the way from the ground to the tropopause. As it would be a large coincidence that both sensors had the same calibration error, the hypothesis of a wrong temperature measurement can be abandoned. It is much more likely that there is a problem in the water vapour measurement. We know that the conditions on the 8 June 2010 were adverse, because the sonde had to transit a 2-km thick mixed phase cloud before reaching the cirrus level and because of the slightly rainy ground conditions.

The following is speculative, but very likely: The SnowWhite inlet has a baffle, which is intended to keep stray light and hydrometeors away from the chilled mirror. However, if a supercooled precipitation drop falling out of the mixed phase cloud were to hit the baffle, it would immediately freeze. The household data of the sonde show that the housing of the instrument (and hence the baffle) during that particular flight was 4 K warmer than ambient in the altitude range 8–15 km. Reason is that the housing is heated by the Peltier element warm side, and even more so by an ohmic heating, which switches on under conditions of supersaturation in order to avoid condensation within the flume. The assumed ice particle would then evaporate slowly and moisten the incoming air flow. Assuming that the ambient gas phase is in equilibrium with ice and the apparent supersaturation of 30 % is due to evaporation of a frozen droplet on the baffle, we estimate from a simple mass balance the droplet size to be of the order of 1 mm in order to supply the air stream with $\Delta RH_{ice} = +30$ % for the whole time needed to traverse the cirrus layer. A phenomenon that might be taken as argument against this explanation is that SnowWhite does show a steep gradient when passing from the troposphere into the stratosphere (Fig. 5b), as it would be a strange coincidence if the frozen droplet would evaporate exactly at the tropopause. However, at the tropopause the controller switches the ohmic heating off (the household data even show that the housing becomes colder than ambient), and therefore the forced evaporation of the

Balloon-borne match measurements

A. Cirisan et al.

Title Page

Abstract

Introduction

Conclusions

References

Tables

Figures

I ◀

▶ I

◀

▶

Back

Close

Full Screen / Esc

Printer-friendly Version

Interactive Discussion



frozen droplet becomes suppressed in the same moment when ambient conditions become dry. Alternatively, already in the boundary layer a rain drop (several millimetre) may have collided with the baffle, slowly evaporating all the way to the tropopause. In Payerne ground conditions were dry, so this may explain the difference between both stations.

Although we do not know exactly what really happened, this explanation is unfortunately very likely. This finding is significant and questions the accuracy of this and all similar humidity measurements. It calls for in-flight checks or calibrations of hygrometers under the extreme humidity conditions in the upper troposphere or at least for critical design reviews to avoid contamination.

5 Conclusions

The occurrence of cirrus clouds and dehydration by sedimenting ice particles determine the water vapour budget and the radiative balance in the upper troposphere. To improve our understanding of the time evolution and life cycle of cirrus clouds in mid-latitudes, we introduce a cloud tracing or “match technique”. A Lagrangian measurement with one fixed and one mobile radiosonde station, supported by a comprehensive microphysical modeling approach, enables us to analyze changes in an air mass occurring within 1–3 h in particle backscatter and relative humidity with respect to ice. This allows determining the occurrence and evolution of ice supersaturation inside and around mid-latitude cirrus. Here we present the first results of match flights performed on 8 June 2010 over Switzerland. A comparison of measured and modeled values reveals that:

1. The underlying regional weather forecast model COSMO-7 data show a timing error of a passing warming phase by about 30 min, which needs to be corrected in order to understand the cloud measurements.

Follow-up investigations are highly desirable, including matches with more favorable wind shear conditions and also studies with cloud-resolving 2-D or 3-D models to fully capitalize on the “match” measurement technique.

Acknowledgements. We gratefully acknowledge funding by COST and GAW-CH: within COST (European Cooperation in Science and Technology) the Match forecasts and measurements were supported by the Swiss State Secretariat for Education and Research (SER-No. C08.0037, Lagrangian Measurements and Modeling of Cirrus Clouds (LAMMOC)) under Action ES0604 “Atmospheric Water Vapour in the Climate System (WaVaCS)”. Within the “Swiss GAW (GAW-CH) Programme 2010–2013” a large part of the data evaluation and simulation was performed as part of the project “Assessment of high altitude cloud characteristics by in-situ and remote sensing techniques”. One of us (TP) was Visiting Scientist with the Cooperative Institute for Research in Environmental Sciences (CIRES) and hosted by the Chemical Sciences Division of NOAA Earth System Research Laboratory (Boulder, CO), and gratefully acknowledges fruitful scientific discussions with Drs. David Fahey, Ru-Shan Gao, Karen Rosenlof, Dan Murphy and A. R. Ravishankara, as well as by Eric Jensen from NASA Ames. We also want to thank Andrew Gettelman from NCAR and Ulrike Lohmann from ETH Zurich for help by reading the original manuscript as well as Michael Sprenger, Daniel Lüthi and Hans Richner from ETH Zurich for introducing and help with a balloon trajectory model, providing COSMO data and radar and ground station data, respectively. Finally, we thank Rolf Maag from Meteolabor (Wetzikon) for support with the SnowWhite sensors.

References

- Bartels-Rausch, T., Bergeron, V., Cartwright, J. H. E., Escribano, R., Finney, J. L., Grothe, H., Gutierrez, P. J., Haapala, J., Kuhs, W. F., Pettersson, J. B. C., Price, S. D., Sainz-Diaz, C. I., Stokes, D. J., Strazzulla, G., Thomson, E. S., and Trinks, H.: Uras-Aytemiz, N.: Ice structures, patterns, and processes: A view across the icefields, *Revs. Mod. Phys.*, 84, 885–944, doi:10.1103/RevModPhys.84.885, 2012. 25452
- Bohren, C. F. and Huffman, D.: Absorption and scattering of light by small particles, New York, Wiley-Interscience, 530 pp., 1983. 25428
- Brabec, M., Wienhold, F. G., Luo, B. P., Vömel, H., Immler, F., Steiner, P., Hausammann, E., Weers, U., and Peter, T.: Particle backscatter and relative humidity measured across cirrus

Balloon-borne match measurements

A. Cirisan et al.

Title Page

Abstract

Introduction

Conclusions

References

Tables

Figures

◀

▶

◀

▶

Back

Close

Full Screen / Esc

Printer-friendly Version

Interactive Discussion



Balloon-borne match measurements

A. Cirisan et al.

Title Page

Abstract

Introduction

Conclusions

References

Tables

Figures

◀

▶

◀

▶

Back

Close

Full Screen / Esc

Printer-friendly Version

Interactive Discussion



clouds and comparison with microphysical cirrus modelling, *Atmos. Chem. Phys.*, 12, 9135–9148, doi:10.5194/acp-12-9135-2012, 2012. 25426, 25428, 25434, 25438

Chen, T., Rossow, W., and Zhang, Y.: Radiative Effects of Cloud-Type Variations, *J. Climate*, 13, 264–286, 2000. 25419

5 Comstock, J., Ackerman, T., and Turner, D.: Evidence of high ice supersaturation in cirrus clouds using ARM Raman lidar measurements, *Geophys. Res. Lett.*, 31, L11106, doi:10.1029/2004GL019705, 2004. 25420

Corti, T. and Peter, T.: A simple model for cloud radiative forcing, *Atmos. Chem. Phys.*, 9, 5751–5758, doi:10.5194/acp-9-5751-2009, 2009. 25419

10 DeMott, P., Cziczko, D., Prenni, A., Murphy, D., Kreidenweis, S., Thomson, D., Borys, R., and Rogers, D.: Measurements of the concentration and composition of nuclei for cirrus formation, *Proc. Natl. Acad. Sci. USA*, 100, 14655–14660, 2003. 25420, 25448

DeMott, P., Prenni, A. J., Liu, X., Kreidenweis, S. M., Petters, M. D., Twohy, C. H., Richardson, M. S., Eidhammer, T., and Rogers, D. C.: Predicting global atmospheric ice nuclei distributions and their impacts on climate, *Proc. Natl. Acad. Sci.*, 107, 11217–11222, 2010. 25419

15 Dionisi, D., Keckhut, P., Hoareau, C., Montoux, N., and Congeduti, F.: Cirrus crystal fall velocity estimates using the Match method with ground-based lidars: first investigation through a case study, *Atmos. Meas. Tech.*, 6, 457–470, doi:10.5194/amt-6-457-2013, 2013. 25422

Engel, I.: Trajectory Modelling of Match Balloon Soundings for Cirrus Cloud Characterisation, Diploma thesis, University of Münster, Faculty of Geosciences, Institute of Landscape Ecology, <http://www.uni-muenster.de/Klima/lehre/diplomarbeiten.shtml>, 2009. 25426, 25467

20 Engel, I., Luo, B. P., Pitts, M. C., Poole, L. R., Hoyle, C. R., Groß, J.-U., Dörnbrack, A., and Peter, T.: Heterogeneous formation of polar stratospheric clouds – Part 2: Nucleation of ice on synoptic scales, *Atmos. Chem. Phys. Discuss.*, 13, 8831–8872, doi:10.5194/acpd-13-8831-2013, 2013. 25426, 25427, 25446, 25447

25 Fahey, D., Gao, R., and Möhler, O.: Summary of the AquaVIT Water Vapor intercomparison: Static Experiments, https://aquavit.icg.kfa-juelich.de/WhitePaper/AquaVITWhitePaper_Final_23Oct2009_6MB.pdf, 2009. 25420

Field, P. R., Heymsfield, A. J., and Bansemer, A.: A Test of Ice Self-Collection Kernels Using Aircraft Data, *J. Atmos. Sci.*, 63, 651–666, 2006. 25422

30 Fritts, D. C. and Alexander, M. J.: Gravity wave dynamics and effects in the middle atmosphere, *Rev. Geophys.*, 41, 1003, doi:10.1029/2001RG000106, 2003. 25439

Balloon-borne match
measurements

A. Cirisan et al.

Title Page

Abstract

Introduction

Conclusions

References

Tables

Figures

◀

▶

◀

▶

Back

Close

Full Screen / Esc

Printer-friendly Version

Interactive Discussion



- Fu, Q.: A new parameterization of an asymmetry factor of cirrus clouds for climate models, *J. Atmos. Sci.*, 64, 4140–4150, 2007. 25428
- Fueglistaler, S., Luo, B. P., Buss, S., Wernli, H., Voigt, C., Müller, M., Neuber, R., Hostetler, C. A., Poole, L. R., Flentje, H., Fahey, D. W., Northway, M. J., and Peter, T.: Large NAT particle formation by mother clouds: Analysis of SOLVE/THESEO-2000 observations, *Geophys. Res. Lett.*, 29, 1610, doi:10.1029/2001GL014548, 2002. 25421
- Fujiwara, M., Shiotani, M., Hasebe, F., Vömel, H., Oltmans, S. J., Ruppert, P. W., Horinouchi, T., and Tsuda, T.: Performance of the meteorolabor “Snow White” chilledmirror hygrometer in the tropical troposphere: Comparisons with the Vaisala RS80 A/H-Humicap sensors, *J. Atmos. Ocean. Technol.*, 20, 1534–1542, 2003. 25425
- Fusina, F. and Spichtinger, P.: Cirrus clouds triggered by radiation, a multiscale phenomenon, *Atmos. Chem. Phys.*, 10, 5179–5190, 2010, <http://www.atmos-chem-phys.net/10/5179/2010/>. 25419
- Fusina, F., Spichtinger, P., and Lohmann, U.: The impact of ice supersaturated regions and thin cirrus on radiation in the mid latitudes, *J. Geophys. Res.*, 112, D24S14, doi:10.1029/2007JD008449, 2007. 25419
- Gallice, A., Wienhold, F. G., Hoyle, C. R., Immler, F., and Peter, T., Modeling the ascent of sounding balloons: derivation of the vertical air motion, *Atmos. Meas. Tech.*, 4, 2235–2253, doi:10.5194/amt-4-2235-2011, 2011. 25439
- Gettelman, A., Fetzer, E., Eldering, A., and Irion, F.: The global distribution of supersaturation in the upper troposphere from the Atmospheric Infrared Sounder, *J. Clim.*, 19, 6089–6103, 2006. 25420
- Gierens, K. and Spichtinger, P.: On the size distribution of ice-supersaturated regions in the upper troposphere and lowermost stratosphere, *Ann. Geophys.*, 18, 499–504, doi:10.1007/s00585-000-0499-7, 2000. 25420
- Gierens, K. M., Monier, M., and Gayet, J.-F.: The deposition coefficient and its role for cirrus clouds, *J. Geophys. Res.*, 108, 4069, doi:10.1029/2001JD001558, 2003. 25443
- Gultepe, I. and Starr, D. O.: Dynamical Structure and Turbulence in Cirrus Clouds: Aircraft Observations during FIRE, *J. Atmos. Sci.*, 52, 4159–4182, 1995. 25422
- Hasebe, F., Fujiwara, M., Nishi, N., Shiotani, M., Vömel, H., Oltmans, S., Takashima, H., Saraspriya, S., Komala, N., and Inai, Y.: In situ observations of dehydrated air parcels advected horizontally in the Tropical Tropopause Layer of the western Pacific, *Atmos. Chem. Phys.*, 7, 803–813, doi:10.5194/acp-7-803-2007, 2007. 25422

Balloon-borne match measurements

A. Cirisan et al.

Title Page

Abstract

Introduction

Conclusions

References

Tables

Figures

◀

▶

◀

▶

Back

Close

Full Screen / Esc

Printer-friendly Version

Interactive Discussion



- Houze, R.: Cloud Dynamics, Academic Press, San Diego, CA, USA, 573 pp., 1993. 25432
- Hoyle, C., Luo, B. P., and Peter, T.: The origin of high ice crystal number densities in cirrus clouds, *J. Atmos. Sci.*, 62, 2568–2579, 2005. 25419, 25426, 25438, 25439, 25440
- Inai, Y.: Cold trap dehydration in the tropical tropopause layer estimated from the water vapor match, Ph.D. thesis, Grad. School of Environ. Sci., Hokkaido Univ., Sapporo, Japan, 2010. 25422
- Jensen, E. and Toon, O.: Ice nucleatin in the upper troposphere: Sensitivity to aerosol number density, temperature, and cooling rate, *Geophys. Res. Lett.*, 21, 2019–2022, 1994. 25419
- Jensen, E., Smith, J., Pfister, L., Pittman, J., Weinstock, E., Sayres, D., Herman, R., Troy, R., Rosenlof, K., Thompson, T., Fridlind, A., Hudson, P., Cziczo, D., Heymsfield, A., Schmitt, C., and Wilson, J.: Ice supersaturations exceeding 100 % for cirrus formation and dehydration, *Atmos. Chem. Phys.*, 5, 851–862, doi:10.5194/acp-5-851-2005, 2005. 25420
- Koop, T., Luo, B. P., Tsias, A., and Peter, T.: Water activity as the determinant for homogeneous ice nucleation in aqueous solutions, *Nature*, 406, 611–614, 2000. 25420, 25427, 25436
- Krämer, M., Schiller, C., Afchine, A., Bauer, R., Gensch, I., Mangold, A., Schlicht, S., Spelten, N., Sitnikov, N., Borrmann, S., de Reus, M., and Spichtinger, P.: Ice supersaturations and cirrus cloud crystal numbers, *Atmos. Chem. Phys.*, 9, 3505–3522, 2009, <http://www.atmos-chem-phys.net/9/3505/2009/>. 25420
- Krieger, U., Mössinger, J., Luo, B., Weers, U., and Peter, T.: Measurement of the Refractive Indices of $\text{H}_2\text{SO}_4\text{-HNO}_3\text{-H}_2\text{O}$ Solutions to Stratospheric Temperatures, *Appl. Opt.*, 39, 3691–3703, doi:10.1364/AO.39.003691, 2000. 25428
- Lin, R.-F., Starr, D. O. C., DeMott, P. J., Cotton, R., Sassen, K., Jensen, E., Kärcher, B., and Liu, X.: Cirrus parcel model comparison project phase 1: The critical components to simulate cirrus initiation explicitly, *J. Atmos. Sci.*, 59, 2305–2329, 2002. 25443
- Luo, B. P., Voigt, C., Fueglistaler, S., and Peter, T.: Extreme NAT supersaturations in mountain wave ice PSCs: A clue to NAT formation, *J. Geophys. Res.*, 108, 4441, doi:10.1029/2002JD003104, 2003. 25426
- Lynch, D., Sassen, K., Starr, D., and Stephens, G. (Eds.): *Cirrus*, Oxford University Press, USA, 2002. 25419
- MacKenzie, A. R. and Haynes, P. H.: The influence of surface kinetics on the growth of stratospheric ice crystals, *J. Geophys. Res.*, 97, 8057–8064, 1992. 25443

Balloon-borne match measurements

A. Cirisan et al.

Title Page

Abstract

Introduction

Conclusions

References

Tables

Figures

◀

▶

◀

▶

Back

Close

Full Screen / Esc

Printer-friendly Version

Interactive Discussion



Magee, N., Moyle, A. M., and Lamb, D.: Experimental determination of the deposition coefficient of small cirrus-like ice crystals near -50 deg C., *Geophys. Res. Lett.*, 33, L17813, doi:10.1029/2006GL026665, 2006. 25443, 25446, 25451

Marcolli, C., Gedamke, S., Peter, T., and Zobrist, B.: Efficiency of immersion mode ice nucleation on surrogates of mineral dust, *Atmos. Chem. Phys.*, 7, 5081–5091, doi:10.5194/acp-7-5081-2007, 2007. 25427, 25447, 25448

Marshall, J. H. and Dobbie, S.: The effects of wind shear on cirrus: A large-eddy model and radar case-study, *Q. J. R. Meteorol. Soc.*, 131, 2937–2955, doi:10.1256/qj.04.122., 2005. 25419

Mason, B.: The role of clouds in the radiative balance of the atmosphere and their effects on climate, *Contemp. Phys.*, 43, 1–11, doi:10.1080/00107510110084075, 2002. 25419

Mishchenko, M.: Light scattering by randomly oriented axially symmetric particles, *J. Opt. Soc. Am.*, 8, 871–882, 1991. 25427, 25428, 25468

Murphy, D. M. and Koop, T.: Review of the vapour pressures of ice and supercooled water for atmospheric applications, *Q. J. Roy. Meteor. Soc.*, 131, 1565, doi:10.1256/qj.04.94, 2005. 25447

Nelson, J.: Growth mechanisms to explain the primary and secondary habits of snow crystals, *Philosophical Magazine A*, 81, 2337–2373, 2001.

Nousiainen, T. and McFarquhar, G.: Light scattering by quasi-spherical ice crystals, *J. Atmos. Sci.*, 61, 2229–2248, 2004. 25428

Ovarlez, J. P. v. V., Sachse, G., Vay, S., Schlager, H., and Ovarlez, H.: Comparison of water vapor measurements from POLINAT 2 with ECMWF analyses in high humidity conditions, *J. Geophys. Res.*, 105, 3737–3744, 2000. 25420

Peter, T., Marcolli, C., Spichtinger, P., Corti, T., Baker, M. B., and Koop, T.: When dry air is too humid, *Science*, 314 (5804), 1399–1400, 2006. 25420, 25443

Peter, T., M. Krämer, and O. Möhler: Upper tropospheric humidity: A report on an international workshop. SPARC Newsletter, No. 30, SPARC Office, Toronto, Ontario, Canada, 9–15, http://www.sparc-climate.org/fileadmin/customer/6_Publications/Newsletter_PDF/30_SPARCnewsletter_Jan2008.pdf, 2008. 25420, 25443

Pratte, P., van den Bergh, U., Rossi, M. J.: The kinetics of H_2O vapor condensation and evaporation on different types of ice in the range 130–210 K, *J. Phys. Chem. A* 110, 3042–3058, doi:10.1021/jp053974s, 2006. 25451

- Pruppacher, H. and Klett, J.: Microphysics of clouds and precipitation, Kluwer Academic Publisher, 1997. 25444, 25446, 25447
- Rex, M.: Stratosphärische Ozonabbauraten aus den Ozonsondendaten der EASOE-Kampagne, Master's thesis, Georg-August-Universität Göttingen, <http://epic.awi.de/3403/1/Wit9999a.pdf>, 1993. 25421
- Rex, M., Harris, N. R. P., van der Gathen, P., Lehmann, R., Braathen, G. O., Reimer, E., Beck, A., Chipperfield, M. P., Alfier, R., Allaart, M., O'Connor, F., Dier, H., Dorokhov, V., Fast, H., Gil, M., Kyrö, E., Litynska, Z., Mikkelsen, I. S., Molyneux, M. G., Nakane, H., Notholt, J., Rummukainen, M., Viatte, P., and Wenger, J.: Prolonged stratospheric ozone loss in the 1995–96 Arctic winter, *Nature*, 389, 835–838, 1997. 25421
- Rex, M., van der Gathen, P., Braathen, G. O., Harris, N. R. P., Reimer, E., Beck, A., Alfier, R., Krüger-Carstensen, R., Chipperfield, M., de Backer, H., Balis, D., O'Connor, F., Dier, H., Dorokhov, V., Fast, H., Gamma, A., Gil, M., Kyrö, E., Litynska, Z., Mikkelsen, S., Molyneux, M., Murphy, G., Reid, S. J., Rummukainen, M., and Zerefos, C.: Chemical ozone loss in the Arctic winter 1994/95 as determined by the Match technique, *J. Atmos. Chem.*, 32, 35–59, 1999. 25421
- Rosen, J. and Kjöme, N.: Backscattersonde: a new instrument for atmospheric aerosol research, *Applied Optics*, 30, 1552–1561, 1991. 25424
- Sadtchenko, V., Brindza, M., Chonde, M., Palmore, B., Eom, R., The vaporization rate of ice at temperatures near its melting point, *J. Chem. Phys.* 121, 11980–11992, doi:10.1063/1.1817820, 2004. 25451
- Meteolabor, data sheet SnowWhite frostpoint mirror, <http://www.meteolabor.ch/en/meteorological-instruments/radiosondierung-en/>, 2013. 25425
- Skrotzki, J.: High-accuracy multiphase humidity measurements using TDLAS: Application to the investigation of ice growth in simulated cirrus clouds, PhD Thesis, Faculties for the Natural Sciences and for Mathematics, University of Heidelberg, Heidelberg, Germany, 140 pp., <http://archiv.ub.uni-heidelberg.de/volltextserver/13141/>, 2012. 25452
- Soden, B. J.: The impact of tropical convection and cirrus on upper tropospheric humidity: A Lagrangian analysis of satellite measurements, *Geophys. Res. Lett.*, 31, L20104, doi:10.1029/2004GL020980, 2004. 25422
- Solomon, S., Qin, D., Manning, M., Chen, Z., Marquis, M., Averyt, K. B., Tignor, M., and Miller, H. L. (Eds.): *Climate Change 2007: The Physical Science Basis. Contribution of Work-*

Balloon-borne match measurements

A. Cirisan et al.

Title Page

Abstract

Introduction

Conclusions

References

Tables

Figures

◀

▶

◀

▶

Back

Close

Full Screen / Esc

Printer-friendly Version

Interactive Discussion



Balloon-borne match measurements

A. Cirisan et al.

Title Page

Abstract

Introduction

Conclusions

References

Tables

Figures

◀

▶

◀

▶

Back

Close

Full Screen / Esc

Printer-friendly Version

Interactive Discussion



- ing Group I to the Fourth Assessment Report of the Intergovernmental Panel on Climate Change, Cambridge University Press, Cambridge, UK and New York, NY, USA, 2007. 25419
- Spichtinger, P.: Cirrus cloud dynamics –a source for ice supersaturation, Tellus A, revised version, 2013. 25433
- 5 Spichtinger, P. and Gierens, K.: Modelling of cirrus clouds – Part 1a: Model description and validation, Atmos. Chem. Phys., 9, 685–706, doi:10.5194/acp-9-685-2009, 2009a. 25419
- Spichtinger, P., Gierens, K., Leiterer, U., and Dier, H.: Ice supersaturation in the tropopause region over Lindenberg, Germany, Meteorol. Z., 12, 143–156, 2003a. 25420
- Spichtinger, P., Gierens, K., and Read, W.: The global distribution of ice-supersaturated regions as seen by the microwave limb sounder, Quart. J. Roy. Meteorol. Soc., 129, 3391–3410, 10 2003b. 25420
- Spichtinger, P., Gierens, K., and Dörnbrack, A.: Formation of ice supersaturation by mesoscale gravity waves, Atmos. Chem. Phys., 5, 1243–1255, doi:10.5194/acp-5-1243-2005, 2005. 25420
- 15 Stephens, G. L.: The influence of radiative transfer on the mass and heat budgets of ice crystals falling in the atmosphere, J. Atmos. Sci., 40, 1729–1739, 1983. 25443
- von der Gathen, P., Rex, M., Harris, N. R. P., Lucic, D., Knudsen, B. M., Braathen, G. O., Debacker, H., Fabian, R., Fast, H., Gil, M., Kyrö, E., Mikkelsen, I. S., Rummukainen, M., Stähelin, J., and Varotsos, C.: Observational evidence for chemical ozone depletion over the Arctic in winter 1991–92, Nature, 375, 131–134, 1995. 25421
- 20 Vömel, H., David, D., and Smith, K.: Accuracy of tropospheric and stratospheric water vapor measurements by cryogenic frost point hygrometer: Instrumental details and observations, J. Geophys. Res., 112, D08305, doi:10.1029/2006JD007224, 2007. 25420
- Wernli, H. and Davies, H.: A Lagrangian-based analysis of extratropical cyclones. I: The method and some applications, Q. J. Roy. Meteor. Soc., 123, 467–489, 1997. 25426
- 25 Wienhold, F. G., COBALD Data Sheet, http://www.iac.ethz.ch/groups/peter/research/Balloon_soundings/COBALD_sensor, 2012. 25424
- Wood, S. E., Baker, M. B., and Calhoun, D.: New model for the vapor growth of hexagonal ice crystals in the atmosphere, J. Geophys. Res., 106, 4845–4870, doi:10.1029/2000JD900338, 2001. 25443
- 30 Zobrist, B., Koop, T., Luo, B. P., Marcolli, C., and Peter, T.: Heterogeneous ice nucleation rate coefficient of water droplets coated by a nonadecanol monolayer, J. Phys. Chem. C., 111, 2149–2155, doi:10.1021/jp066080w, 2007. 25447

Balloon-borne match measurements

A. Cirisan et al.

Table 2. Relative error (in %) given by M in Eq. (3) between backscatter measurement and model results for the run with the best fluctuation member using the clear, cloudy or “all sky” scenarios. Microphysical conditions are unity mass accommodation coefficient ($\alpha=1$) and the absence of ice nuclei ($n_{\text{IN}}=0$).

	COSMO without fluct.	COSMO with superimposed fluct.		
		clear sky	cloudy sky	“all sky”
Payerne	–51	–15	0	–21
Zurich	–76	–17	–9	–31

Title Page

Abstract

Introduction

Conclusions

References

Tables

Figures

◀

▶

◀

▶

Back

Close

Full Screen / Esc

Printer-friendly Version

Interactive Discussion



Balloon-borne match measurements

A. Cirisan et al.

Table 4. Relative error (in %) given by M in Eq. (3) between backscatter measurement and model results for the runs with the best fluctuation member for the “all sky” scenario. Two values of the mass accommodation coefficient ($\alpha = 1$ and $f(\text{RH})$) and two values for heterogeneous ice nuclei ($n_{\text{IN}} = 0$ and 10 L^{-1}) are indicated.

	COSMO	COSMO with superimposed “all sky” fluctuations			
	without fluct. $\alpha = 1, \text{IN} = 0$	$\alpha = 1$ $\text{IN} = 0$	$\alpha = f(\text{RH})$ $\text{IN} = 0$	$\alpha = 1$ $\text{IN} = 10 \text{ L}^{-1}$	$\alpha = f(\text{RH})$ $\text{IN} = 10 \text{ L}^{-1}$
Payerne	−51	−21	+5	+1	−12
Zurich	−76	−31	+2	−8	−8

Title Page

Abstract

Introduction

Conclusions

References

Tables

Figures

◀

▶

◀

▶

Back

Close

Full Screen / Esc

Printer-friendly Version

Interactive Discussion



Balloon-borne match measurements

A. Cirisan et al.

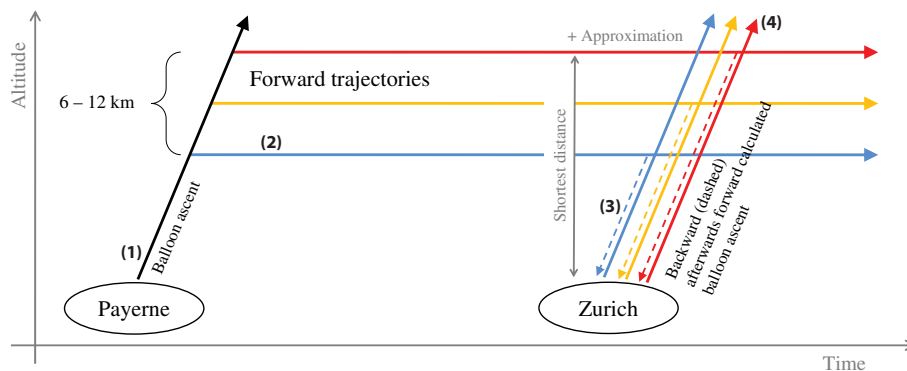


Fig. 1. Schematic representation of match procedure. (1) Calculate balloon ascent trajectory from Payerne. (2) Determine the direction of 15 air parcel forward trajectories, starting at points in the cirrus region represented here by three colored horizontal arrows. (3) Calculate backward balloon tracks in the vicinity of the downstream location (close to Zurich) associated with each of the air parcel trajectories. (4) Calculate balloon ascent trajectories from each of the locations in the vicinity of Zurich to estimate the match quality at higher levels (Engel, 2009).

Title Page

Abstract

Introduction

Conclusions

References

Tables

Figures

◀

▶

◀

▶

Back

Close

Full Screen / Esc

Printer-friendly Version

Interactive Discussion



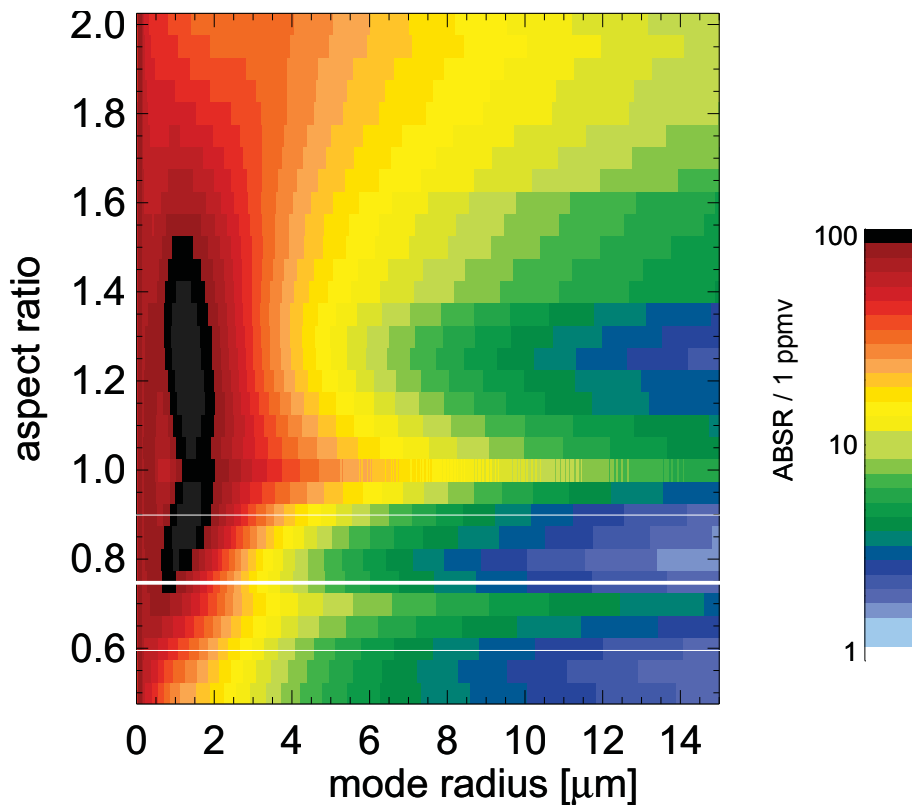


Fig. 2. Colour diagram depicting aerosol backscatter at 870 nm calculated by means of the T-matrix method (Mishchenko, 1991) for spheroids as function of aspect ratio A and equivalent sphere radius r . The figure assumes 1 ppmv of H_2O condensed in the ice phase. Results for other condensed phase mixing ratios can be obtained by linear scaling. Thick white line: $A = 0.75$ assumed here. Thin white lines: $\pm 20\%$ deviations.

Balloon-borne match measurements

A. Cirisan et al.

Title Page

Abstract Introduction

Conclusions References

Tables Figures

◀ ▶

◀ ▶

Back Close

Full Screen / Esc

Printer-friendly Version

Interactive Discussion



Balloon-borne match measurements

A. Cirisan et al.

Title Page

Abstract

Introduction

Conclusions

References

Tables

Figures

◀

▶

◀

▶

Back

Close

Full Screen / Esc

Printer-friendly Version

Interactive Discussion

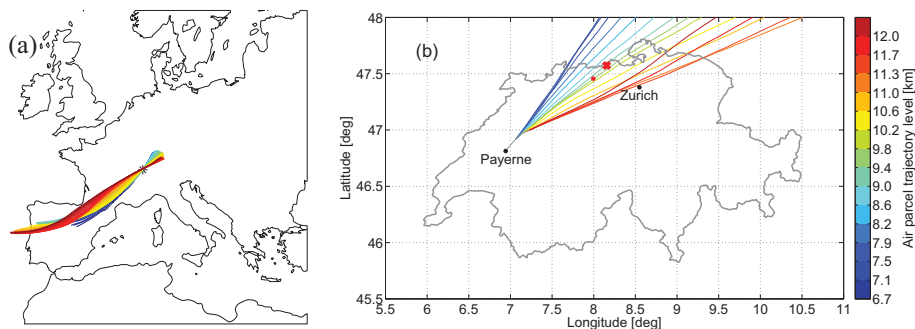


Fig. 3. (a) Ensemble of trajectories calculated with the COSMO-7 analysis fields backward and forward in time calculated by LAGRANTO from the track of the balloon started from Payerne (8 June 2010, 20:04 UTC), showing the evolution from 20 h upstream to 4 h downstream of Payerne. (b) Air parcel trajectories for different altitude levels calculated using COSMO-2 analysis in combination with the GPS data of the balloon ascent in Payerne. Red dot shows the downstream launch site (47.46° N, 7.99° E) fitting the trajectory at 9.4 km altitude that gives the best match distance (about 1.5 h downstream of Payerne) presented with a red cross (47.57° N, 8.15° E).

Balloon-borne match measurements

A. Cirisan et al.

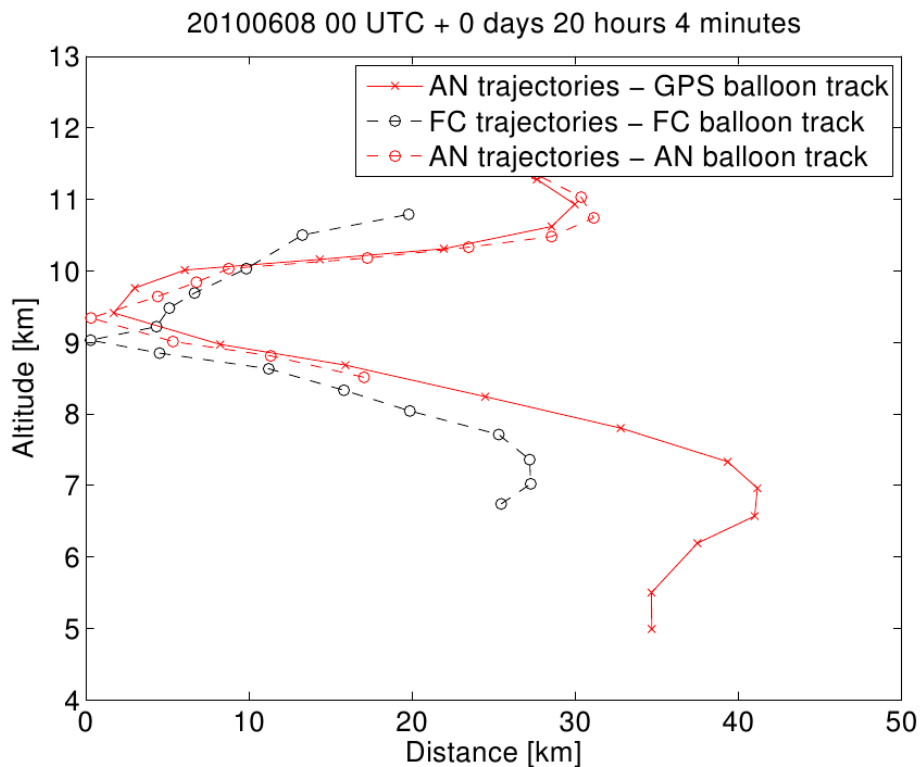


Fig. 4. Match distances between air parcel and the balloon trajectories based on different data sets. Forward trajectories are computed with COSMO-2 forecast (FC) and analysis (AN), respectively, at the same potential temperature level and point in time.

Balloon-borne match measurements

A. Cirisan et al.

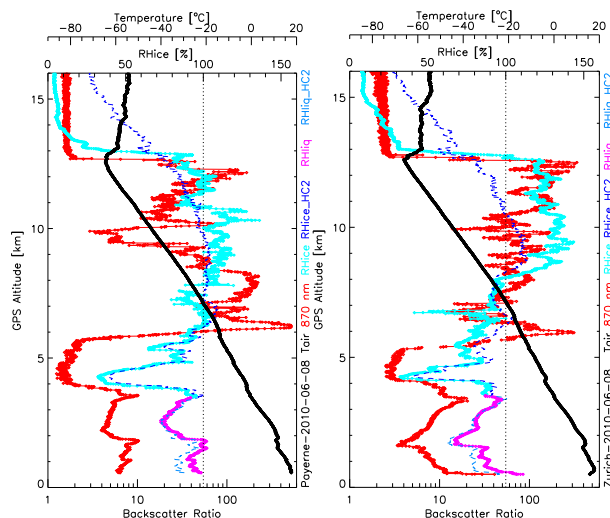


Fig. 5. Soundings on 8 June 2010 launched from Payerne at 20:04 UTC (left) and from the vicinity of Zurich at 21:28 UTC (right). Thick black line: temperature profile. Red: measured backscatter ratio at 870 nm wavelength. Cyan: RH_{ice} calculated from SnowWhite frost/dew point measurement by assuming solid condensate on the SnowWhite mirror above 7 km and liquid condensate below 7 km. Magenta: RH_{liq} calculated from SnowWhite dew point measurement. Thin dashed dark and light blue line: RH_{ice} and RH_{liq} , respectively, measured by HC2 Humicap capacitive polymer sensor. Note that the apparent supersaturation with respect to liquid water in the boundary layer suggested by SnowWhite is caused by partial evaporation of hydrometeors, while they enter the heated instrument inlet (see text).

Title Page

Abstract

Introduction

Conclusions

References

Tables

Figures

◀

▶

◀

▶

Back

Close

Full Screen / Esc

Printer-friendly Version

Interactive Discussion



Balloon-borne match measurements

A. Cirisan et al.

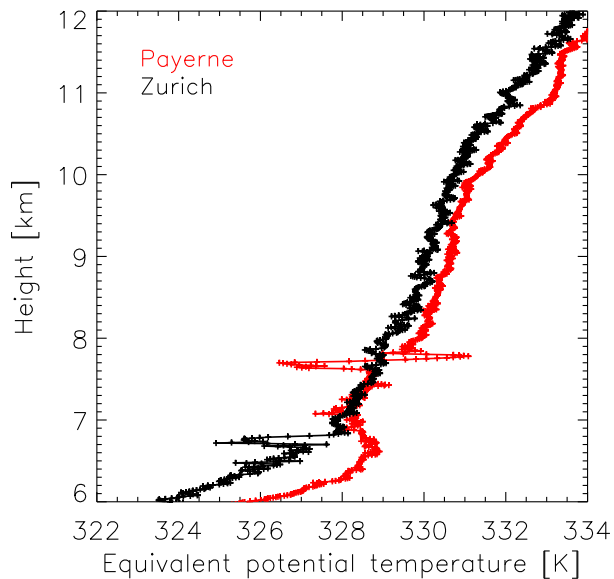


Fig. 6. Equivalent potential temperature profile θ_{eq} calculated from Payerne and Zurich soundings showing the presence of potentially unstable layers indicative of convective activity.

[Title Page](#)[Abstract](#)[Introduction](#)[Conclusions](#)[References](#)[Tables](#)[Figures](#)[◀](#)[▶](#)[◀](#)[▶](#)[Back](#)[Close](#)[Full Screen / Esc](#)[Printer-friendly Version](#)[Interactive Discussion](#)

Balloon-borne match measurements

A. Cirisan et al.

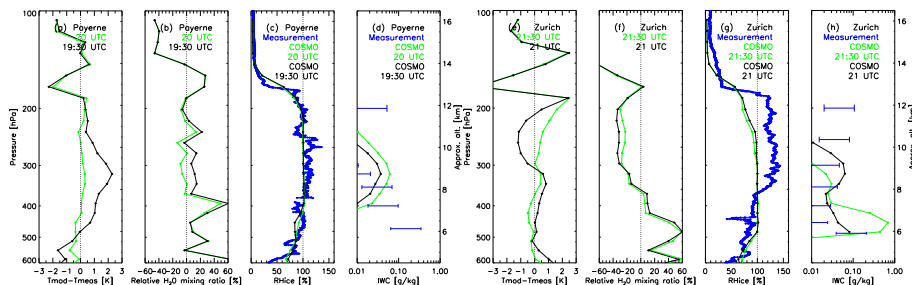


Fig. 7. Validation of COSMO-7 analysis data with the sonde measurements over Payerne (upper row) and Zurich (lower row) along the balloon track (green points) or half an hour upstream (black points): **(a)** and **(e)** temperature difference between COSMO and measured data; **(b)** and **(f)** percentage difference between model and measurement in water mixing ratio $(\chi_{w,mod} - \chi_{w,meas})/\chi_{w,meas}$; **(c)** and **(g)** relative humidity with respect to ice RH_{ice} obtained from the measurement data (blue) and COSMO data (black and green); **(d)** and **(h)** same for the ice water content (IWC) with blue bars showing uncertainty range in IWC estimated from the COBALD data.

Title Page

Abstract

Introduction

Conclusions

References

Tables

Figures

◀

▶

◀

▶

Back

Close

Full Screen / Esc

Printer-friendly Version

Interactive Discussion



Balloon-borne match measurements

A. Cirisan et al.

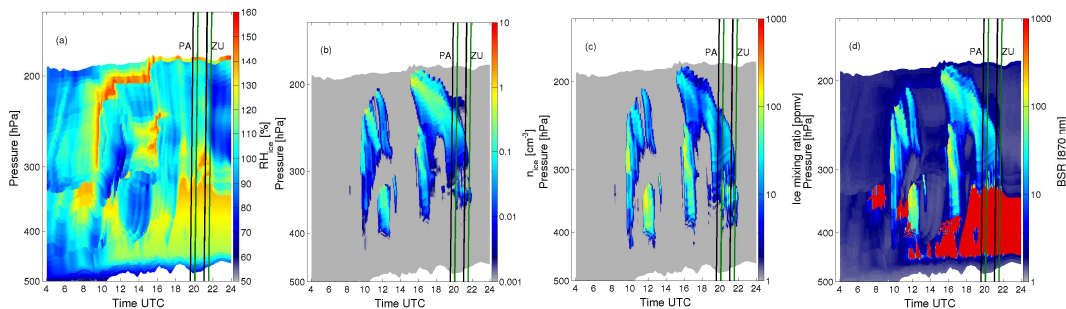


Fig. 9. Detailed microphysics runs with column spectral model based on the original COSMO-7 analysis fields. **(a)** Relative humidity with respect to ice; **(b)** ice crystal number density; **(c)** ice mixing ratio (defined as number of water molecules condensed in ice per number of air molecules) and **(d)** aerosol backscatter ratio (870 nm wavelength). Green lines: flight tracks of balloons launched from Payerne (“PA”) and Zurich (“ZU”). Black lines: positions shifted by half hour upstream (to compensate for a COSMO warming phase error). In **(d)**, $BSR < 5$ indicate aerosols with various amounts of H_2O uptake (at different relative humidities), $5 < BSR \leq 100$ are cirrus clouds, and deep red color indicates mixed phase clouds.

Balloon-borne match measurements

A. Cirisan et al.

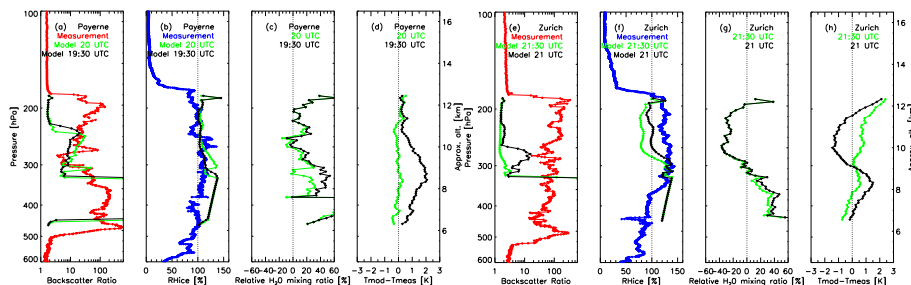


Fig. 10. Comparison of the measurements with the model results calculated from trajectories in Fig. 9 based on original COSMO-7 fields at the time of measurements (green lines) and half an hour upstream (black lines). Upper row: Payerne sounding. Lower panel: Zurich sounding. Quantities shown: **(a, e)** BSR at 870 nm; **(b, f)** RH_{ice} ; **(c, g)** percentage difference between model and measurement in water mixing ratio, $(\chi_{w, mod} - \chi_{w, meas}) / \chi_{w, meas}$; **(d, h)** difference in temperature between model and measurement.

Title Page

Abstract

Introduction

Conclusions

References

Tables

Figures

◀

▶

◀

▶

Back

Close

Full Screen / Esc

Printer-friendly Version

Interactive Discussion



Balloon-borne match measurements

A. Cirisan et al.

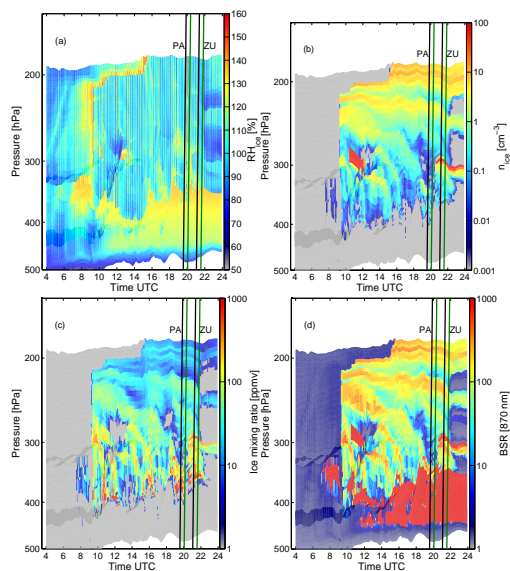


Fig. 11. Detailed microphysics runs with column spectral model based on the original COSMO-7 analysis fields with superimposed small-scale temperature fluctuations: **(a)** Relative humidity with respect to ice; **(b)** ice crystal number density; **(c)** ice mixing ratio (defined as number of water molecules condensed in ice per number of air molecules); **(d)** aerosol backscatter ratio (870 nm wavelength). Green lines: flight tracks of balloons launched from Payerne (“PA”) and Zurich (“ZU”). Black lines: positions shifted by half hour upstream (to compensate for a COSMO warming phase error). Thin vertical stripes in RH_{ice} reveal the $(dT/dt)_{ss}$ superimposed on the adiabatic trajectories based on COSMO fields. All sky conditions are assumed for the small-scale temperature fluctuations, mass accommodation coefficient of H_2O on ice is a function of RH and no heterogeneous nucleation is assumed (see text).

Balloon-borne match measurements

A. Cirisan et al.

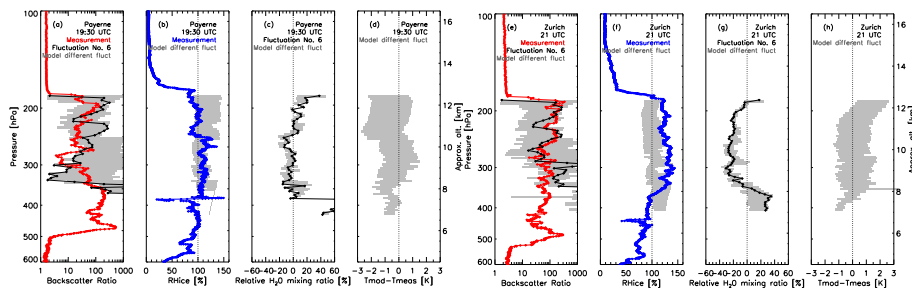


Fig. 12. Comparison of sonde measurements of BSR at 870 nm (**a**, **e**), red lines), RH_{ice} (**b**, **f**, blue lines), relative H_2O mixing ratio (**c**, **g**) and $T_{mod}-T_{meas}$ in Payerne (upper row) and Zurich (lower row) with the model results based on COSMO-7 trajectories with superimposed small-scale temperature fluctuations (“all sky” scenario). Black lines: best fluctuation member. Gray shaded area: results for all 10 ensemble members with randomly chosen fluctuations. Comparison is made half an hour upstream of the exact measurement time using adiabatic trajectories with latent heat corrections from ZOMM (see Sect. 3.5.1), and $\alpha = f(RH_{ice})$ (see Sect. 3.5.2), but no heterogeneous nucleation.

Title Page

Abstract

Introduction

Conclusions

References

Tables

Figures

◀

▶

◀

▶

Back

Close

Full Screen / Esc

Printer-friendly Version

Interactive Discussion



Balloon-borne match measurements

A. Cirisan et al.

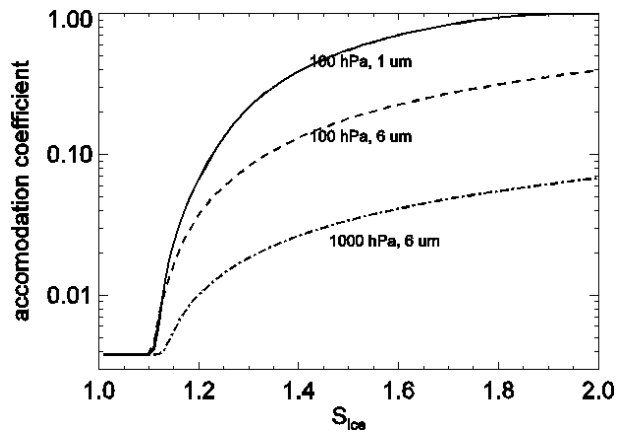


Fig. 13. Mass accommodation coefficient as a function of saturation ratio over ice surface for different pressures and layer thicknesses.